Diffraction excitation of protons on protons and deuterons at high energies and small momentum transfers

S. V. Mukhin

Joint Institute for Nuclear Research, Dubna

V. A. Tsarev

P. N. Lebedev Physics Institute, USSR Academy of Sciences, Moscow
Fiz. Elem. Chastits At. Yadra 8, 989–1055 (September–October 1977)

The results are presented of measurements of the cross sections of diffraction dissociation of protons on hydrogen and deuterium made with the Dubna jet target at the Fermi National Accelerator Laboratory in the United States. Theoretical models of diffraction dissociation are discussed and compared with experiment.

PACS numbers: 13.85.Hd, 12.40.Pp

INTRODUCTION

It was noted long ago that certain inelastic hadron processes exhibit a remarkable similarity to elastic scattering: Their cross sections are almost independent of the energy; in the t channel, exchange with the vacuum quantum numbers predominates; basically the processes involve small momentum transfer, so that the differential cross sections have sharp peaks in the forward direction; there is a large rapidity interval between the groups of particles in the final state; and the particle and antiparticle cross sections are approximately equal.

Processes of this type are usually called diffraction dissociation processes or inelastic diffraction scattering, and the properties listed above usually serve as the empirical definition of diffraction dissociation. A well-known example of diffraction dissociation is the excitation of the states $J^P(M)$: $1/2^+(1400)$ and $5/2^+(1688)$ in proton–proton scattering.

The phenomenon of inelastic diffraction scattering has already been studied experimentally and theoretically for about two decades. However, until recently the range of energies in which the measurements were made was small and restricted to 10–30 GeV. On the basis of data then available, one could believe that diffraction dissociation occupies a very modest place among the competing processes and is due principally to the excitation of hadrons in low-mass resonance states. Investigations in recent years have radically changed the picture and stimulated greater interest in diffraction dissociation. The new accelerators have led to a significant extension of the energy range available for experiments. An important result of this was the discovery of the diffraction excitation of hadrons in states with large mass.[1] The currently available data suggest that there are no restrictions on the mass of the diffraction-excited system provided the colliding particles have sufficient energy. Thus, at high energies diffraction dissociation is one of the most important channels with a contribution to the total cross section comparable with the elastic-scattering contribution.

At higher energies, it is also possible to separate out more fully the diffraction mechanisms and thus study them in more detail. The properties found at low masses can be used as criteria for identifying inelastic diffraction processes in the more general case when a continuum of large-mass states is formed. Let us consider, for example, the reaction of quasielastic scattering of hadron h_1 on hadron h_2:

$$h_1 + h_2 \to X + h_2, \tag{1}$$

in which one of the hadrons does not change its state and the other is transformed into the hadronic system X. The rapidity distribution of the particles for this case (Fig. 1a) has, in contrast to the nondiffraction process with its more uniform distribution, a large interval between the groups of particles. It is important to note that the secondary particles produced by the dissociation of one of the hadrons are distributed in an interval $\sim \ln(M_X^2/m^2)$, and the reliable identification of a diffraction event requires a sufficiently high initial energy.

Besides reactions of the type (1), in which one of the incident hadrons is excited, one can also have reactions of the type

$$h_1 + h_2 \to X_1 + X_2 \tag{2}$$

and

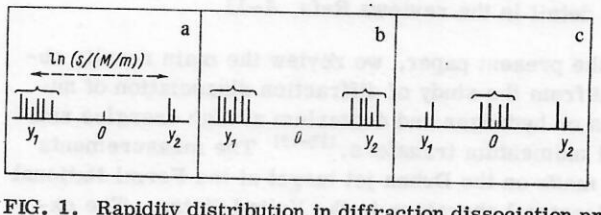

FIG. 1. Rapidity distribution in diffraction dissociation processes: a) single dissociation; b) double dissociation; c) double pomeron exchange.

 0090-4759/77/0805-0403$02.80

$$h_1+h_2 \to h_1+h_2+X. \quad (3)$$

The rapidity distributions in these processes are shown schematically in Figs. 1b and 1c.

There are two main theoretical approaches to diffraction dissociation. One of them is related to the t-channel picture of the scattering, and it distinguishes the exchange nature of the interaction. The basic entities of the theory in this case are the leading singularities of the scattering amplitude in the complex plane of the angular momentum j: the Regge poles and branch points related to them. In the framework of this approach, diffraction dissociation processes are defined as inelastic processes that proceed through the exchange of a Pomeranchuk singularity situated near $j=1$ at $t=0$. Since the same singularity is assumed to be responsible for elastic diffraction scattering, this automatically ensures fulfillment of the diffraction dissociation properties listed above. Unfortunately, this definition is too summary (or at least, it is at present) since the concept of a Pomeranchuk singularity is used at different times and by different authors to mean variously a pole, a branch point, a complex-conjugate pair of poles or branch points, etc. Nevertheless, the formalism of Regge theory even in its simplest form with a pole pomeron is very convenient for phenomenological investigations of diffraction dissociation.

Diffraction dissociation can be analyzed by a different approach which presupposes an intimate analogy between hadron diffraction processes and optics. The initial hadron is regarded as a superposition of different "virtual" many-particle states. If the initial energy is sufficiently high, the interaction with the target can lead, as a result of collision of the "virtual" particles, to transitions to many open channels. This results in the absorption of the incident wave and, just as in optics in the case of scattering on an absorbing object, diffraction (shadow) scattering occurs with characteristic diffraction minima and maxima. If all the components of the incident hadron are absorbed to the same extent, elastic diffraction scattering results. If the different components are absorbed differently (in optics, this corresponds to scattering on a polarized target), the wave is "rearranged" and the diffraction leads to a new state of the hadron differing from the initial state.[2,3] This is the diffraction dissociation. Some of the individual features of diffraction phenomena are reproduced better in the optical (s-channel) approach and others in the t-channel approach. Models that pay regard to the requirements of both channels have the greatest success.

The literature on diffraction dissociation is given in more detail in the reviews Refs. 4–11.

In the present paper, we review the main results obtained from the study of diffraction dissociation of nucleons on hydrogen and deuterium at high energies and small momentum transfers.[12–18] The measurements were made on the Dubna jet target at the Fermi National Accelerator Laboratory in the United States. The experiments detected the slow recoil particles (protons or deuterons) and measured the inclusive cross section of "single" dissociation (1) of protons.

In Sec. 1, we consider the arrangement of the experiment, give the results of the measurements, and compare them with the results obtained by other methods. Section 2 is devoted to a theoretical discussion of diffraction dissociation and confrontation of the predictions of the theoretical models with the experiments. In the conclusions, we summarize the main results of the work and discuss possible directions of development of diffraction dissociation investigations with the jet target.

Before we turn to presentation of the results, we should like to point out that the method employed has important advantages that were exploited in the experimental program.

1. The good mass resolution offered hope of determining at high energies the resonance structure hitherto observed only at low energies and not so far observed experimentally at high energies.

2. The use of the internal target made it possible to measure simultaneously (in one session) the reaction cross sections in a wide energy range (in the present case from 8 to 400 GeV). A high accuracy was achieved in determining the initial momentum, and the systematic error resulting from separate measurements at different energies was eliminated. This is important for many problems such as: testing of scaling, separation of various three-reggeon contributions, study of the contraction of the forward peaks, determination of the relative importance of the resonances and the nonresonance background at different energies, and separation of the purely diffraction contribution and determination of its role in the increase in the total cross section.

3. The detection of the slow recoil particles made it possible to measure the diffraction dissociation cross section in the region of the smallest momentum transfers. This region is of particular interest for contemporary theory in connection with the separation at small $|t|$ of the three-pomeron coupling and the cross section of the pomeron–proton interaction. It is also important to establish whether the diffraction dissociation cross section has a minimum as $|t| \to 0$, as predicted in various theoretical schemes.

4. The measurement in a single experiment of the excitation cross sections at both low and high masses with good mass resolution eliminated the error in the relative normalization of the cross sections, which is important for testing the duality hypothesis for inclusive processes.

5. The use of a deuterium target had not only methodological advantages, which we consider below, but also a number of physical advantages. Because the deuteron has zero isotopic spin, one can separate more reliably the diffraction mechanisms since in the t channel only exchange with zero isospin is allowed. The nuclear target also opens up the basic possibility of studying the spacetime development of hadronic processes and measuring the cross section of interaction of the unstable system X with nucleons.

1. METHODS AND RESULTS OF THE EXPERIMENTAL INVESTIGATION OF INELASTIC DIFFRACTION SCATTERING OF PROTONS ON PROTONS AND DEUTERONS

Dependence of the mass resolution on the kinematics and accuracy in the determination of the measured quantities

Considering a process of the type

$$a+b \to c+d \quad (1+2 \to 3+4), \tag{4}$$

where a is the incident particle and b is the target, one can consider diffraction dissociation of only the incident particle:

$$a+b \to X_L+b \tag{5}$$

or only the target:

$$a+b \to a+X_T, \tag{6}$$

or the double diffraction dissociation

$$a+b \to X_L+X_T. \tag{7}$$

Choosing the kinematic variables in a definite manner, one can emphasize different aspects of the reactions. For example, taking the variables to be

$$s=(p_1+p_2)^2, \tag{8}$$

i.e., the square of the total cms energy, the Feynman variable x, which is equal to the ratio of the longitudinal momentum component of the detected particle to its maximal value:

$$x=p_\parallel/p_{\max}, \tag{9}$$

and $p_\perp$, the transverse momentum component of the detected particle, we focus our attention on the leading particle. On the other hand, the variable s, the square of the four-momentum transfer

$$t=(p_1-p_3)^2=(p_2-p_4)^2, \tag{10}$$

and M_X^2, the square of the mass of the excited system (the missing mass) emphasize the quasi-two-particle aspect of the reaction.

Considering processes at high energies and small transfers, we write the connection between the two sets of variables in the form

$$M_X^2=s(1-x)+\{m^2-2(p_\perp^2+m^2)(x-1)/x\} \tag{11}$$

or, to a good approximation,

$$1-x\approx(M_X^2-m^2)/s \tag{12}$$

and

$$t=-p_\perp^2/x-m^2(x-1)^2/x. \tag{13}$$

Since x is always near unity in diffraction dissociation, we have

$$t\approx-p_\perp^2. \tag{14}$$

Using (12) and (14), we can find a simple relationship between the invariant differential cross sections expressed in different variables:

$$E\,d\sigma/d^3p=x\,d\sigma/(dx\,dp_\perp^2)=s\,d\sigma/dM_X^2\,dt=d\sigma/dx\,dt. \tag{15}$$

Note that the above kinematic variables are derived from experimentally measured values and the accuracy of their determination depends not only on the choice of the experimental method but also on the type of accelerator used in the experiment.

Currently, only two laboratories (FNAL and CERN) can study diffraction dissociation processes at energies $s\geq 100$ GeV^2. At FNAL, experiments are made on internal and external beams of the accelerator on stationary targets, i.e., in the laboratory coordinate system, whereas at CERN they are made in the center-of-mass system on colliding beams. The differences in the experimental possibilities resulting from operation in the different coordinate systems reduce basically to the following.[19]

1. The missing-mass resolution for colliding and extracted beams in the case of diffraction dissociation of the target (6) depends strongly on the accuracy in the measurement of the momentum of the incident and the detected particle:

$$dM_X^2\approx s\,dp_1/p_1;\quad dM_X^2\approx -s\,dp_3/p_3, \tag{16}$$

while it depends weakly or not at all on the momentum of the target particle:

$$dM_X^2\approx M_X^2\,dp_2/p_2. \tag{17}$$

2. The energy loss of the incident particle required for excitation of the target to a state with mass M_X when an extracted beam is used as $2E_1/m$ times greater than when colliding beams are used, and the scattering angle of the particle is that many times smaller. Therefore, to achieve the same mass resolution in experiments with colliding beams the momentum resolution must be $2E_1/m$ times better, while in experiments with extracted beams this requirement is imposed on the angular resolution.

3. In the case of diffraction dissociation (5) of the incident particle, we have

$$dM_X^2\approx M_X^2\,dp_1/p_1;\quad dM_X^2\approx M_X^2\,dp_3/p_3. \tag{18}$$

Comparing (16) and (18), we see that when the recoil particle is detected an accuracy greater by s/M_X^2 times is achieved in the determination of the missing mass. Note that in the case of colliding beams the concept of the incident particle and the target particle more or less dissolves and reduces to considering which of the beams has greater influence on the missing-mass resolution.

Thus, for purely kinematic reasons the inclusive distributions obtained on the colliding beams at CERN have missing-mass resolution that is more than an order of magnitude worse.

4. The minimal value of the square of the momentum transfer amenable to measurement in the case of diffraction dissociation of the target particle can be estimated from the relation

$$-t = p_1 p_3 \theta_{\min}^2, \tag{19}$$

where $\theta_{\min}$ is the minimal measurable scattering angle.

On the colliding beams at CERN the size of the vacuum chamber and the circulating beam lead to $\theta_{\min} \approx 35$ mrad.

As the energy of the circulating beams increases from 11.8 to 31.4 GeV/c, the value of $-t_{\min}$ varies in the interval 0.15–1.15 (GeV/c)^2. For extracted beams one usually has $\theta_{\min} \approx 1.5$ mrad, which for $p_3 \approx p_1 \approx 300$ GeV/c gives $-t_{\min} = 0.20$ (GeV/c)^2. At the same time, if the recoil particle is detected, $t_{\min}$ does not depend on the energy of the incident particle since

$$-t = 2mT_3 \approx p_3^2, \tag{20}$$

but is completely determined by the instrumental possibilities. By means of semiconductor detectors one can detect recoil particles with kinetic energy of order 100 keV, i.e., one can have $-t_{\min} = 0.0002$ (GeV/c)^2.

Aspects of the method of recoil-particle detection in the investigation of inelastic processes

Before we turn to considering the measurement of the inelastic interaction cross sections, let us consider in more detail the method of detection of the recoil particles that makes possible the most accurate measurement in the kinematic region of particular interest in connection with diffraction dissociation. The main difficulty in detecting recoil particles electronically at small transfers arises from the uncertainties in the measurement of the emission angle of the particles and their energy due to multiple scattering and ionization loss in the target. These effects have hitherto presented great experimental difficulties when the method is used with extracted beams.

A brilliant solution to this problem was found in 1963 by workers at the High Energy Laboratory at Dubna.[20,21] Passing the internal beam of the accelerator many times through a thin (~1 μ) film $(CH_2)_n$ target, they reduced the above uncertainties to a minimum but retained a large aperture of the apparatus.

In the proposed method, the range of measured t is determined by the chosen detection system, i.e., by the detectors, while the limit $t_{\min}$ is determined by the same uncertainties as above, but now in a thin target. Development of the method showed that semiconductor detectors are the best for detecting recoil particles at small momentum transfers; they have a high energy resolution, ~50 keV, and replaced the previously used

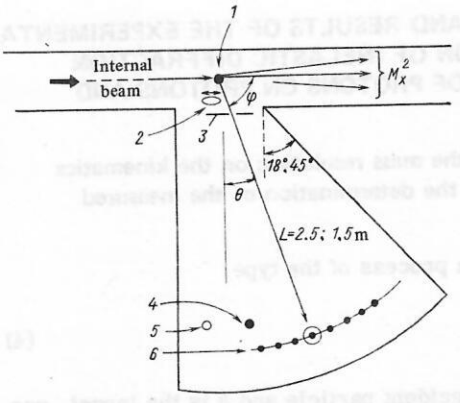

FIG. 2. Arrangement of experimental apparatus on the FNAL internal beam: 1) jet target; 2) movable shield; 3) slit; 4) monitor at +4°; 5) monitor at −2°; 6) carriage.

nuclear photoemulsions.[22,23] Later, the film target was replaced by the jet target developed at the same laboratory. The principle of operation of this target is described in detail in Refs. 24–27. If pure hydrogen or deuterium gases are used, it is then no longer necessary to make difference measurements to subtract the background of quasielastic interactions on carbon. Because of the low density ~$3 \cdot 10^{-7}$ g/cm^3 of the jet, the target imposes virtually no restrictions on $t_{\min}$.

The method was used in a series of experiments on elastic pp and pd scattering at small momentum transfers, first in the Dubna synchrophasotron, and then in the accelerator at Serpukhov. It proved itself a splendid tool for studying processes of this kind.

At the beginning of 1972, when the new 400-GeV accelerator was completed at the FNAL, this method formed the basis of a Soviet–American collaboration between Dubna, FNAL, Rockefeller University, and the University of Rochester. A new jet target developed at Dubna was adapted for fitting onto the new detector; together with the detecting and measuring apparatus it served as the basis for the first experiments on this accelerator to study elastic and inelastic pp and pd interactions.[12,28–31] A review of the elastic scattering results can be found in Refs. 32 and 33.

In the present paper, we discuss the experiments on inelastic interactions. Basically, the experiment for the inelastic interactions is similar to the one used to measure elastic scattering. The scattered particles resulting from the interaction of the internal beam of the accelerator with the gas jet are detected by telescopes of semiconductor detectors (Fig. 2). The detectors are arranged on a remotely controlled movable carriage within the beam pipe, which is directly joined to the main vacuum of the accelerator. For normalization of the results, one of the detectors is placed outside the carriage and used as a monitor to detect elastic interactions at the constant angle 4°.

The jet target is operated in a pulsed regime with pulse duration 300 msec and density ~$3 \cdot 10^{-7}$ g/cm^3 of the jet. The possibility of firing the target at any time during the accelerator cycle makes it possible to collect

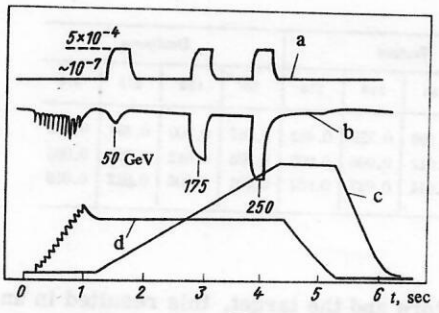

FIG. 3. Operation of the FNAL accelerator in the 300-GeV regime during a cycle. The time and duration of firing of the jet target are revealed by the monitor of intensity and pressure losses in the chamber; a) pressure in the target chamber; b) intensity loss monitor; c) magnetic field strength; d) intensity of accelerator beam.

statistical material at any given energy in the range from the injection energy to the maximal energy of the accelerator. However, the background conditions associated with the beam loss during the injection time and the initial stage of acceleration made it difficult to work at energies below 40 GeV. For better statistical reliability of the results, the measurements were made at four fixed energies: 50, 150, 270, and 370 GeV, with, as a rule, the target fired three times in one cycle of the accelerator (Fig. 3). The minimal time interval between two pulses of the target was 1 sec, this being basically determined by the rate of evacuation of the residual gas. The apparatus used in the experiments is described in more detail in Ref. 34.

Let us consider briefly the measurement of the inelastic events. The differential cross sections of inelastic pp and pd interactions are measured as functions of the scattering angle $\theta = (90° - \varphi)$, the kinetic energy T of the recoil particles, and the momentum p of the primary beam. The square of the mass of the excited state is determined by

$$M_X^2 \approx m^2 + 2p\sqrt{|t|}\,[\sin\theta - (1 + M/p)\sqrt{|t|}\,2M]\,. \qquad (21)$$

where m is the proton mass, M is the mass of the recoil particle, and $t = 2MT$.

In inelastic interactions, in contrast to elastic interactions, the rigid connection between the momentum transfer and the scattering angle is lost. As a result, the energy spectrum of the detected recoil particles does not have the peak characteristic of elastic scattering. Thus, one lacks one of the principal criteria for separating the effect from the background.

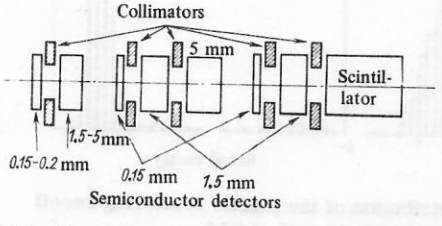

FIG. 4. Components of detector telescopes.

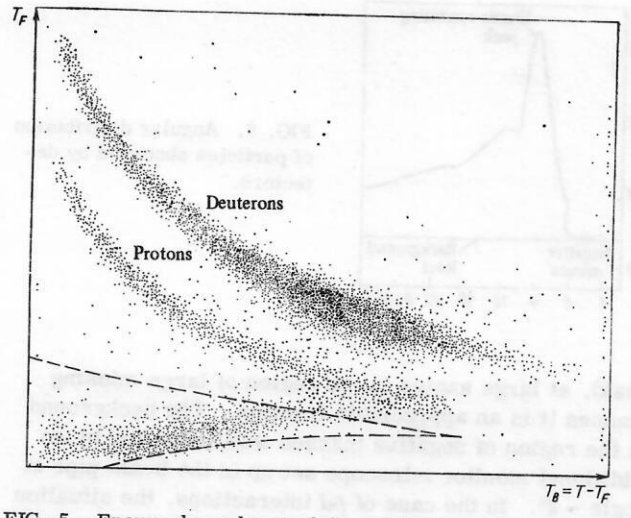

FIG. 5. Energy dependence of the distribution of events identified in the first, T_F, and second, T_B, detectors of the telescope for the case of elastic scattering of deuterons. The dashed curve is the proton collimator curve.

Let us consider what the background consists of and the measures one can take to suppress or determine it. Roughly speaking, the background can be divided into the following components:

a) the "room" background—the proton component of the radiation from the accelerator itself;

b) recoil particles produced as a result of the interaction of the primary beam with the target that reach a detector as a result of multiple scattering on different parts of the apparatus;

c) recoil particles that pass through the detector with energy greater than the detectable energy;

d) protons formed as a result of the breakup of deuterons used in a deuterium target.

By using telescopes made of two or more detectors (Fig. 4), one can, by measuring dT/dx in the first detector, separate the background of types c) and d) from the effect in a subsequent analysis.

The completeness of the separation of protons, deuterons, and particles that pass through the detectors by means of telescopes consisting of two detectors is well illustrated in Fig. 5. In this method of detection, the thickness of the first detector determines the minimal value of the measured kinetic energy. Thus, if the detector is 150-μ thick, then $T_{\min} = 4.0$ MeV for protons and $T_{\min} = 5.3$ MeV for deuterons.

Use of telescopes made obvious the advantage of using deuterons as target, the backgrounds of type a) and b) being appreciably less for them. To reduce the background of type b), lead collimators (horizontal and vertical) were set up in the beam pipe.

The number of events counted by a detector telescope is shown as a function of its angular position for fixed t in Fig. 6 for pp interactions. Although the number of counts in the region of negative masses for $\theta < 0$ is very low (three orders of magnitude lower than at the elastic

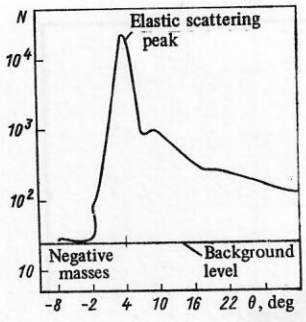

FIG. 6. Angular distribution of particles observed by detectors.

peak), at large angles in the region of large missing masses it is an appreciable fraction. The background in the region of negative masses was measured by an additional monitor telescope set up in the beam pipe at angle $-2°$. In the case of pd interactions, the situation with regard to the background was improved by an order of magnitude, as we have already mentioned. Estimates were made under the assumption that the background was independent of the angle.

To test the validity of this assumption and measure directly the background in the beam pipe at a distance of about 20 cm from the target, we set up a movable shield (see Fig. 2) prepared from a "heavy" metal containing 90% tungsten. During the experiments, the background was periodically measured by using the shield to cover the region of interaction of the beam and the target as seen from the detectors. The shield was a cylinder with rounded ends of diameter 12 mm and length 40 mm. The experimental test showed that the background from the shield itself did not exceed 5% of the measured background. The first results have confirmed a weak angular dependence of the background; the evaluation of the data is continuing.

To conclude this section, let us consider questions associated with the resolution of the apparatus and the determination of the effective area of the detectors.

Differentiating the expression (21), we readily obtain the dependence of the mass resolution on the accuracy with which the measured quantities are determined:

$$(dM_X^2)_\theta \approx 2p\sqrt{|t|}\,d\theta; \quad (22)$$

$$(dM_X^2)_p \approx (M_X^2 - m^2)\,dp/p; \quad (23)$$

$$(dM_X^2)_t \approx |(M_X^2 - m^2)/t - p/M - 1|\,dt. \quad (24)$$

The uncertainty in the missing mass associated with the measurement of the momentum transfer by the semiconductor detectors does not exceed 0.06 GeV/c^2. Since the region of masses accessible to measurement at fixed momentum transfer expands in proportion to the energy p, by choosing the gate width for the accelerator energy during the collection of experimental data it was possible to ensure the necessary accuracy in the mass resolution. The main factor determining the mass resolution in these experiments was the angular resolution. The width of the accelerator tunnel at FNAL in which the measuring apparatus was placed did not make it possible to have a path greater than 2.5 m between the target and the detectors, so that, for the final

TABLE I.

p_{lab}, GeV/c	Protons				Deuterons			
	50	150	270	370	50	150	270	370
$(dM_X^2)_\theta$, GeV^2	0.066	0.199	0.359	0.492	0.067	0.200	0.361	0.495
$(dM_X^2)_p$, GeV^2	0.035	0.012	0.006	0.005	0.035	0.012	0.006	0.005
$(dM_X^2)_t$, GeV^2	0.003	0.014	0.027	0.037	0.001	0.006	0.012	0.018

sizes of the detectors and the target, this resulted in an angular indeterminacy of ± 3 mrad for a jet target measuring ± 6 mm at the half-height of its distribution, with detector diameter $\phi \approx 10$ mm for a flight path $L = 2.5$ m and $\phi \approx 5$ mm for a path $L = 1.5$ m in the case of a beam pipe with wide opening angle. In Table I, we give the partial mass resolutions as functions of the energy of the primary beam for $M_X^2 = 2$ GeV^2, $d\theta = \pm 3$ mrad, $dp = \pm 1.5$ GeV, and $dt = \pm 2 \cdot 10^{-4}$ (GeV/c)^2 for proton and deuterium targets.

One of the possible ways of improving the angular resolution is to use a movable shield in the form of a slit that cuts out the jet as seen from the detectors (see Fig. 2). Figure 7 shows the cutoff effect. In this way, it was possible to improve the resolution by a factor of 2. The slit method proved suitable only for measurements in the region of small masses, where the elastic scattering peak can be seen in the energy spectrum of the detectors and used for monitoring. At the Internal Target Laboratory at FNAL, where the experiments with the jet target are made, a new measuring pavilion has been constructed permitting an increase of the experimental flight path L to 7.5 m. A further proposal has been made[35] for a considerable improvement in the resolution. The effect is achieved by magnetic focusing into a "point" of the recoil particles emitted at one angle and measurement of the position of this "point" by means of a position-sensitive semiconductor detector. Thus, a connection is established between the position of focusing and the value of the missing mass at fixed momentum transfer.

In experiments to investigate elastic processes, collimators with openings that determine the working area of the detectors were set up in front of the detectors. Since the elastic-scattering recoil particles have maximal energy at a given angle, it is easy to calculate the thickness of the collimator that stops such particles. As the missing mass is increased in measurements of

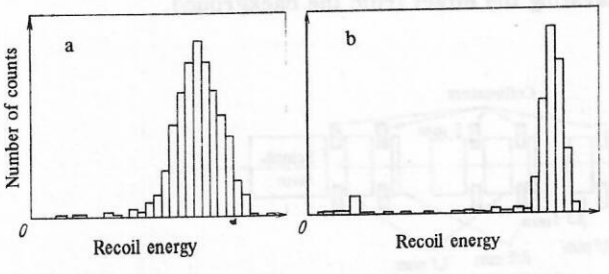

FIG. 7. Energy distribution of the elastic scattering recoil particles: a) without shield; b) with shield.

diffraction dissociation processes, the difference between the energy of the measured recoil particle and its maximal possible energy corresponding to elastic scattering increases. At the same time, the necessary thickness of the collimator increases and becomes comparable with the dimensions of its opening, which increases the collimator edge effects and leads to possible distortions of the measured spectra. Incorrect allowance for this effect can explain, for example, the bend toward zero in the t distribution observed in the experiment of Refs. 36 and 37.

One of the possible ways of solving the problem of collimating the working area of the detectors in inelastic-interaction measurements is to set up the collimators between the detectors in the manner shown in Fig. 4. Particles that reach a collimator may, depending on their energy, be stopped or pass right through it. Then, for one and the same energy deposited in the second detector, they may, because of the loss in the collimator, have a smaller signal in the first detector compared with the event particles. As a result, in the distribution shown in Fig. 5, such particles form a "collimator" curve which can be separated from the main curve in a subsequent analysis.

For reliable separation of the two curves, it is sufficient to have comparatively thin collimators, 0.5–1.5 mm, for which the edge effect can be ignored.

Other methods for studying diffraction dissociation

Among other methods, we shall consider briefly only two: the bubble-chamber method used on the extracted beams at FNAL and the spark-spectrometer method used on the colliding beams at CERN. Comparison of the results obtained by means of the jet target and by means of chambers makes it possible to test the correctness of their normalization and, in conjunction with the work at CERN, obtain a general idea about the behavior of the cross sections as the momentum transfer and energy increase.

The use of track detectors, namely Wilson cloud chambers, to study processes with small momentum transfers was proposed at the High Energy Laboratory at Dubna in 1963 (Refs. 20 and 21).

The chambers were introduced in the regime insensitive to relativistic particles and thus separated the nonrelativistic recoil protons and measured their scattering angle and energy (from the range). This method is widely used at the present time in the chamber method to study, for example, diffraction dissociation processes.[38,39] In a bubble chamber with its regime unchanged, a recoil proton is distinguished from other particles by the double ionization and can be reliably measured in the momentum range $0.12 \leqslant p \leqslant 1.4$ GeV/c, and this determines the momentum transfer range in these experiments. The chamber method is distinguished by the possibility of studying the global picture of the process in the case of operation with beams of different particles and the possibility of obtaining the absolute normalization of the measured cross sections.

The majority of the results obtained at CERN for inelastic interaction in the colliding beams at small momentum transfers were obtained using the single-arm spectrometer, this being slightly modified for the various different experiments. One of the latest variants is shown in Fig. 8. The spectrometer consists of two septum magnets, three bending magnets BM 1, 2, 3, a system of 21 magnetostrictive spark chambers, a series of trigger scintillation counters and three gas Čerenkov counters $\check{C}_1$, $\check{C}_2$, $\check{C}_3$.

The range of measured angles is 30–180 mrad, and the error is 0.2 mrad, which corresponds to a ~0.5% uncertainty in the transverse momentum component $p_\perp$. The error in the momentum measurement ranges from 0.6 to 1.1% depending on the angle, and it is this that determines the mass resolution in accordance with (16):

$$dM_X^2 \approx s\, dp_3/p_3 \approx s\, dx. \tag{25}$$

To separate out elastic events, a hodoscope of 38 scintillation counters and six spark chambers is placed on the other side of the spectrometer. The counters over-

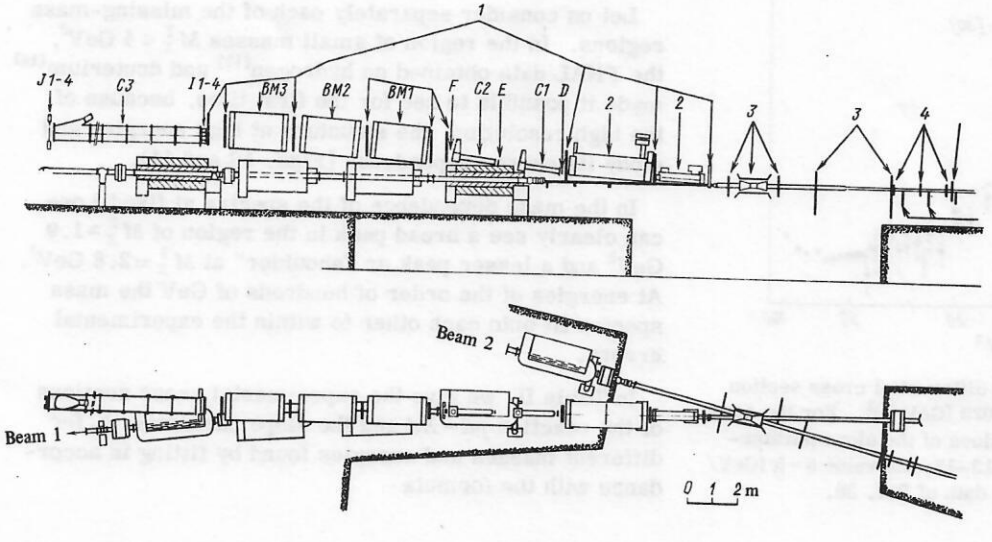

FIG. 8. Arrangement of the CERN single-arm spectrometer: 1) spark chambers; 2) septum magnets; 3) anticoincidence counters; 4) monitor.

lap the angular range from 8 to 250 mrad and have angular resolution 16 mrad. The angle of overlap of the spark chambers in the vertical direction is 10–50 mrad and in the horizontal it is ±20 mrad. Elastic events are distinguished by the collinearity in the vertical plane [with error ±(6–8) mrad] of one charged particle in this telescope and the particle detected by the spectrometer. The region of intersection of the beams is surrounded by a system of counters that cover almost 4π, the signal from these being used to separate the elastic events at large momentum transfers. A more detailed description of the spectrometer can be found in Refs. 40 and 41.

Experimental results

Already the first results of the experiments made by means of the deuterium jet target[13–15] made it possible to combine the previously existing experimental data obtained at CERN (Ref. 1) and FNAL (Refs. 12 and 30) in the region of large and small masses and obtain a general picture of the behavior of the differential cross section as a function of the missing mass (Fig. 9).

It can be seen in Fig. 9 that the cross section at fixed $|t|$ and s has a peak in the region of small masses (at $M_X^2 \approx 1.9$ GeV^2), and then decreases rapidly with increasing M_X^2 (in the region up to $M_X^2 \approx 25$ GeV^2), leveling out then with further increase in M_X^2. Thus, the behavior of the cross sections permits one to divide the mass spectrum into three regions: small, intermediate, and large masses.

Here and in what follows, when comparing the pd and pp data, we shall make the assumption of "nuclear factorization" of the pd cross sections:

$$(d\sigma/dt)^{pd} = (d\sigma/dt)^{pp} F_d(p, t), \tag{26}$$

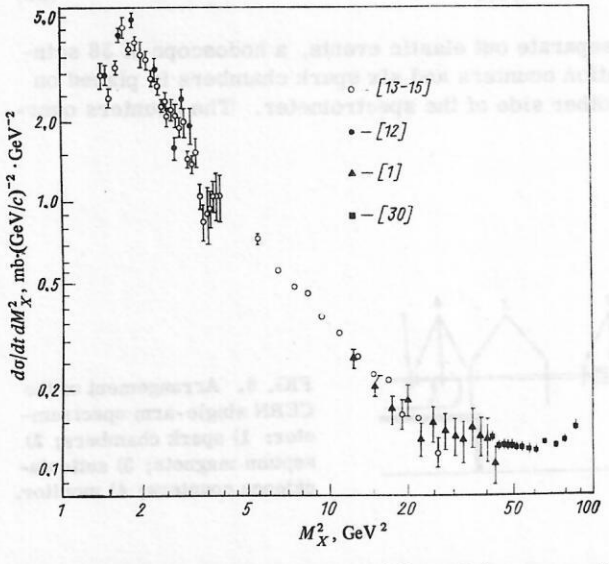

FIG. 9. Dependence of the $pp \to Xp$ differential cross section on M_X^2 for $s = 500$ GeV^2 and $|t| = 0.025$ (GeV/c)^2. For the conversion of the cross sections the values of the slope parameters were taken from Refs. 1, 12, 13–15; the value $b = 5$ (GeV/c)$^{-2}$ was taken for conversion of the data of Ref. 30.

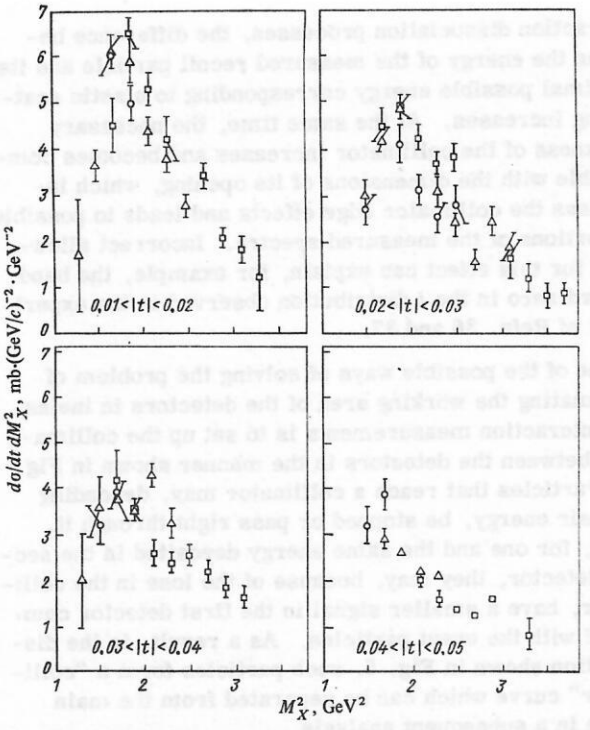

FIG. 10. Mass spectrum of the reaction $pp \to Xp$ in the region of small M_X^2 for different fixed t.

with the coherent factor

$$F_d(p, t) = [\sigma_t^{pd}(p)/\sigma_t^{pp}(p)]^2 |S(t)|^2. \tag{27}$$

In the energy range of the FNAL accelerator, $50 \leqslant p \leqslant 400$ GeV/c, the ratio of the total pp and pd cross sections[42] does not, with an error of order 2%, depend on the energy, and $(\sigma_t^{pd}/\sigma_t^{pp})^2 = 3.6$. In this energy range at small $|t| < 0.12$ (GeV/c)^2 the elastic pd cross section can be well described[34] by means of the form factor

$$|S(t)|^2 = \exp(-b_0|t| + c_0 t^2), \tag{28}$$

where $b_0 = 26.4$ (GeV/c)$^{-2}$ and $c_0 = 62.3$ (GeV/c)$^{-4}$. The ratio of the proton and deuteron cross sections is discussed in more detail in Sec. 2.

Let us consider separately each of the missing-mass regions. In the region of small masses $M_X^2 \leqslant 4$ GeV^2, the FNAL data obtained on hydrogen[12] and deuterium[16] made it possible to see for the first time, because of the high resolution, the structure at high energies and study its energy dependence (Figs. 10 and 11).

In the mass dependence of the spectra at fixed t one can clearly see a broad peak in the region of $M_X^2 \approx 1.9$ GeV^2 and a lesser peak or "shoulder" at $M_X^2 = 2.8$ GeV^2. At energies of the order of hundreds of GeV the mass spectra fit onto each other to within the experimental errors.

In Table II, we give the experimental cross sections of the reaction $pd \to Xd$ and the slope parameter b_d for different masses and energies found by fitting in accordance with the formula

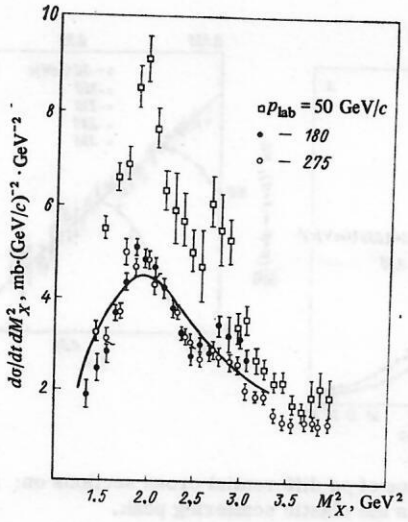

FIG. 11. Differential cross section of $pd \to Xd$ interaction at $t = 0.035$ (GeV/c)^2 and small M_X^2.

$$d\sigma/dt\,dM_X^2 = A\exp[-b_d(|t|-a)+c_0(t^2-a^2)] \qquad (29)$$

for fixed $c_0 = 62.3$ (GeV/c)$^{-4}$ and $a = 0.035$ (GeV/c)^2.

It is interesting to compare the structure obtained in the mass spectrum at high energies with the one observed at low energies.[43–45] Such a comparison[4] is made in Fig. 12. Extrapolation[46] of the data obtained at low energies by means of the relation

$$d\sigma/dt = a(M_X) + b(M_X)\,s^{-q(M_X)}, \qquad (30)$$

to $s \to \infty$ gives values close to the FNAL results. In the same figure, the points are the results of fitting under the assumption of excitation of nucleon isobars on a smoothly varying background. If it is assumed that the background disappears with increasing energy, the excitation cross section of the isobars will be virtually independent of the energy. To illustrate this, in Fig. 13 we show different results[12,14,44–47] on the determination of the t dependence of the cross section for the production of the "isobar" $N^*(1400)$.

TABLE II.

p_{lab}, GeV/c	50		180		275	
M_X^2, GeV^2	$\frac{d\sigma}{dt\,dM_X^2}\Big\|_{t=0.035}$, mb·(GeV/$c$)$^{-2}$·GeV^{-2}	b_d, (GeV/c)$^{-2}$	$\frac{d\sigma}{dt\,dM_X^2}\Big\|_{t=0.035}$, mb·(GeV/$c$)$^{-2}$·GeV^{-2}	b_d, (GeV/c)$^{-2}$	$\frac{d\sigma}{dt\,dM_X^2}\Big\|_{t=0.035}$, mb·(GeV/$c$)$^{-2}$·GeV^{-2}	b_d, (GeV/c)$^{-2}$
1.35	—	37.2±7.2	1.88±0.29	43.6±3.6	—	49.1±2.3
1.45	—		2.47±0.29		3.29±0.24	
1.55	5.55±0.26		2.83±0.20		3.13±0.14	
1.65	6.60±0.23		3.71±0.14		3.75±0.15	
1.75	6.87±0.36	40.1±2.2	4.38±0.15	50.4±1.6	5.01±0.25	48.2±1.7
1.85	8.52±0.39		5.09±0.14		4.67±0.14	
1.95	9.11±0.47		4.86±0.16		4.87±0.15	
2.05	7.65±0.44		4.72±0.23		4.68±0.33	
2.15	6.34±0.40		4.26±0.19		4.37±0.21	
2.25	5.89±0.71	43.4±5.4	3.78±0.16	41.8±2.4	3.74±0.12	43,4±2.4
2.35	5.72±0.47		3.24±0.12		3.18±0.14	
2.45	5.05±0.43		2.78±0.17		3.09±0.11	
2.55	4.74±0.69	41.7±4.4	3.04±0.16	39.9±3.2	2.73±0.12	40,7±2.0
2.65	6.07±0.51		2.85±0.17		2.86±0.16	
2.75	5.48±0.73		3.48±0.19		2.75±0.17	
2.85	5.27±0.45		3.27±0.41		2.64±0.13	
2.95	3.39±0.34		3.22±0.20		2,60±0.16	
3.05	3.59±0.28	36.1±4.1	2.71±0.20		2.04±0.10	38.5±2.8
3.15	2.71±0.30		—		1.87±0.10	
3.25	2.55±0.21		—		1.89±0.15	
3.35	2.23±0.21		—		1.47±0.10	
3.45	2.24±0.25	32.8±4.4			1.38±0.12	35,0±4.5
3.55	1.76±0.22				1.30±0.17	
3.65	1.58±0.20				1.38±0.12	
3.75	1.91±0.41				1.37±0.10	
3.85	2.13±0.37				1.29±0.11	
3.95	1.95±0.38				1.35±0.10	

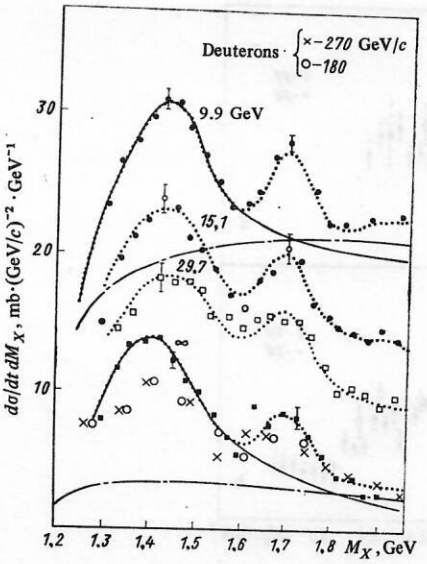

FIG. 12. Comparison of mass spectra for the reaction $pp \to Xp$ obtained at high and low energies. The continuous and the dashed curves correspond to a background of DHD type and polynomial type.

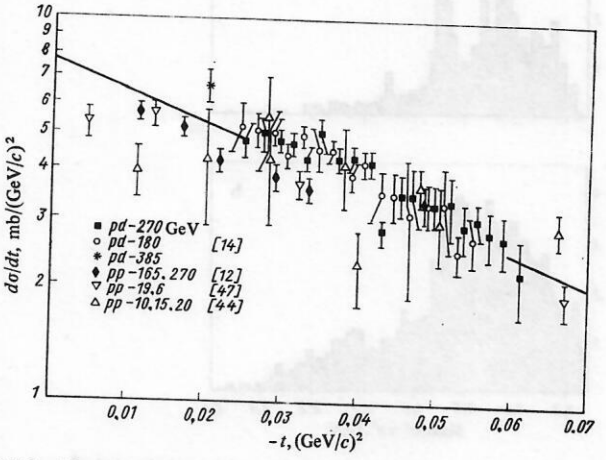

FIG. 13. Comparison of the results of different experiments on the determination of the t dependence of the cross sections for the excitation of the "isobar" $N^*(1400)$.

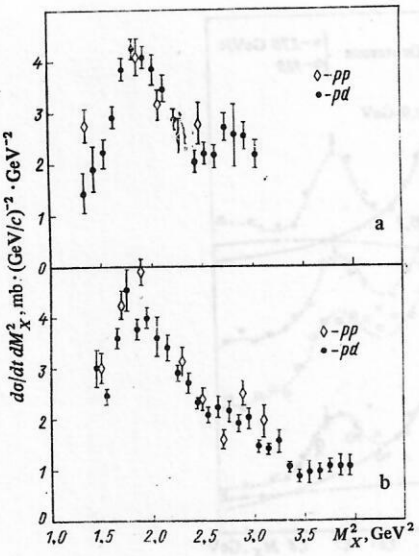

FIG. 14. Comparison of pd cross sections divided by F_d (Ref. 16) and the pp data (Ref. 12): a) for energy 175–180 GeV/c; b) for 260–275 GeV/c.

The good agreement between the pp and pd results obtained at high energies (Fig. 14) shows that the cross section does factorize to within the experimental errors. The structure of the mass spectrum will be discussed in detail below. Here, we merely mention that inclusion of exclusive data makes it possible to understand more fully the structure. In particular, analysis of the $pp \to p(n\pi^+)$ reaction[48] indicates the presence of two components that have different decay angular distributions (Fig. 15). One of the components, which corresponds to isotropic decay for $\theta_J < 0$ in the Jackson coordinate system, has a clearly expressed resonance structure, whereas the second for $\theta_J > 0$ indicates only a broad peak in the region of $M_X \approx 1.4$ GeV.

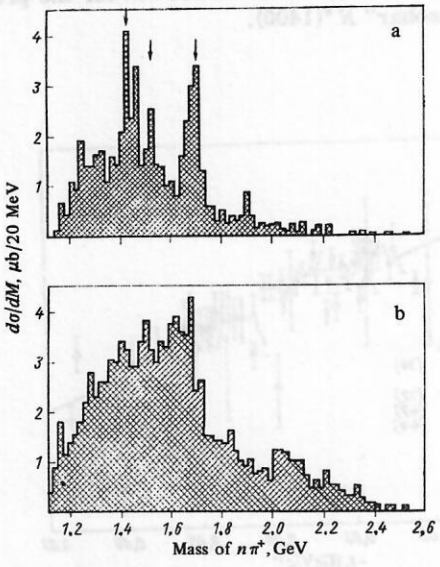

FIG. 15. Mass spectrum of $n\pi^+$ for $-t > 0.05$ (GeV/c)^2 and two ranges of angles in the Jackson coordinate system: a) $\cos\theta_J < 0$; b) $\cos\theta_J > 0$.

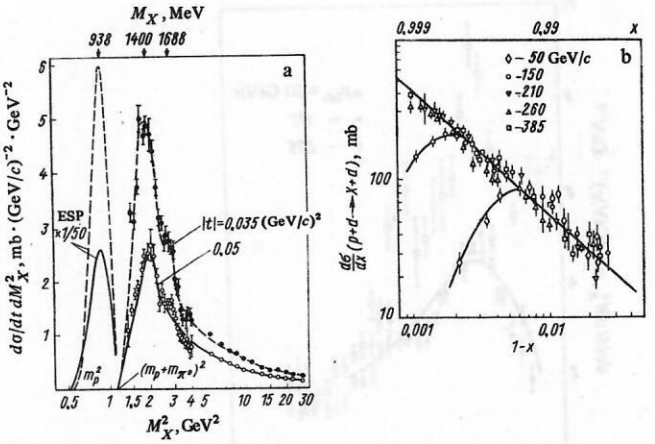

FIG. 16. Dependence of pd differential cross sections on: a) M_X^2, b) $1-x$; ESP is the elastic scattering peak.

Turning to the region of intermediate masses $5 \leq M_X^2 \leq 0.05s$ GeV^2, we note that here the cross section no longer exhibits a resonance structure and decreases rapidly with increasing M_X^2. In Fig. 16, we show $d\sigma/dtdM_X^2$ as a function of M_X^2 for the $pd \to Xd$ reaction at two values of the momentum transfer $|t| = 0.035$ and 0.05 (GeV/c)^2 and $p = 275$ GeV/c (Ref. 17). The data obtained by fitting in accordance with formula (29) with $a = 0.05$ are given in Table III.

Ideas about the important role of three-pomeron exchange in diffraction dissociation lead one to expect a decrease of the cross section in this region as $1/M_X^2$ with increasing mass of the excited system. To test this conclusion, the results obtained were fitted in accordance with the formula

$$d\sigma/dt\,dM_X^2|_{t=0.05} = D(s)/(M_X^2)^{\alpha(s)}. \qquad (31)$$

The results given in Table IV show that $\alpha(s)$ is near unity and hardly depends on s, whereas the dependence of $D(s)$ on s indicates a departure from scaling in this range of energies and masses.

TABLE III.

p_{lab}, GeV/c	150		275		385	
M_X^2, GeV^2	$d\sigma/dtdM_X^2$, mb (GeV/c)$^{-2}$ · GeV^{-2}	b_d, (GeV/c)$^{-2}$	$d\sigma/dtdM_X^2$, mb (GeV/c)$^{-2}$ · GeV^{-2}	b_d, (GeV/c)$^{-2}$	$d\sigma/dtdM_X^2$, mb (GeV/c)$^{-2}$ · GeV^{-2}	b_d, (GeV/c)$^{-2}$
5.5	0.700±0.019	33.5±2.4	0.635±0.025	37.0±3.3		
6.5	0.600±0.010	34.7±0.8	0.538±0.010	32.6±1.3	0.580±0.057	25.1±13.4
7.5	0.528±0.013	30.4±1.1	0.451±0.009	34.0±1.2	0.432±0.010	37.3±1.9
8.5	0.425±0.011	32.9±2.4	0.416±0.015	35.1±1.6	0.364±0.008	32.0±1.6
9.5	0.394±0.007	33.0±0.9	0.340±0.011	35.3±3.1	0.341±0.005	34.6±1.1
11.0	0.335±0.006	30.7±1.0	0.307±0.007	33.8±1.0	0.293±0.006	33.5±1.0
13.0	0.294±0.010	31.5±1.2	0.252±0.015	33.1±4.9	0.229±0.004	32.8±1.6
15.0	0.243±0.020	28.5±2.9	0.217±0.007	33.3±2.9	0.214±0.005	30.5±1.1
17.0	—	—	0.201±0.005	34.3±0.9	0.188±0.005	31.3±1.5
19.0	—	—	0.177±0.011	27.3±8.2	0.167±0.005	35.8±2.8
22.0	—	—	0.154±0.005	31.9±1.1	0.137±0.003	34.8±1.9
26.0	—	—	0.126±0.012	27.7±4.5	0.125±0.003	33.1±1.4
30.0	—	—	—	—	0.109±0.004	33.1±2.1
34.0	—	—	—	—	0.101±0.007	30.5±1.8
38.0	—	—	—	—	0.090±0.020	28.9±8.2

TABLE IV.

p_{lab}, GeV/c	$D(s)$, mb · (GeV/c)$^{-2}$ · GeV^{-2}	$\alpha(s)$	χ^2
150	4.38±0.33	1.068±0.035	1.10
	3.784±0.035	1	1.43
275	3.63±0.019	1.028±0.019	0.83
	3.391±0.030	1	0.93
385	3.19±0.15	1.004±0.017	1.90
	3.157±0.023	1	1.77

The new pd data obtained on the basis of the extensive statistics at FNAL (Ref. 18) in the region $0.02 \leqslant |t| \leqslant 0.18$ (GeV/c)^2 and $122 \leqslant s \leqslant 699$ GeV^2 (Fig. 17) confirm the $1/M_X^2$ dependence and the departure from scaling.

As can be seen in Fig. 18, the new pp data obtained on the colliding beams at CERN at higher energies and larger momentum transfers, $549 \leqslant s \leqslant 1464$ GeV^2, $|t| = 0.25$ (GeV/c)^2 (Ref. 41), also agree well with the $1/M_X^2$ dependence, but do not reveal deviation from scaling within the experimental errors.

So far, comparing the experiments made on protons and deuterons, we have not found any contradictions to the assumption of nuclear factorization of the pd cross sections to within the relative normalization of the cross sections. It is of interest to establish whether this assumption is also true in the region of large masses for $1-x>0.05$, where the slowing down in the decrease of the cross sections with increasing $1-x$ indicates a change in the nature of the processes governing the inelastic scattering.

To answer this question, let us consider Fig. 19, in which we have plotted the latest FNAL results for $pp \to Xp$ at $p=500$ GeV/c (Ref. 49) and $pd \to Xd$ at $p=370$ GeV/c (Ref. 18). Disregarding questions associated with the normalization and the difference in the energies (in both cases, the results are preliminary), we can see that the cross sections behave identically as functions of the mass.

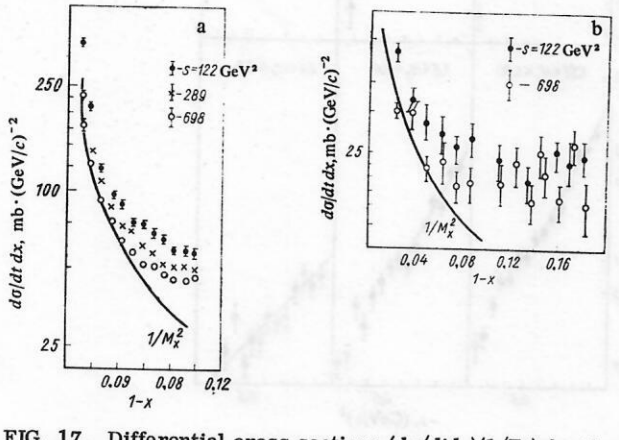

FIG. 17. Differential cross sections $(d\sigma/dtdx)(1/F_d)$ for the reaction $pd \to Xd$ obtained at: a) $t=-0.03$ (GeV/c)^2; b) $t=-0.13$ (GeV/c)^2.

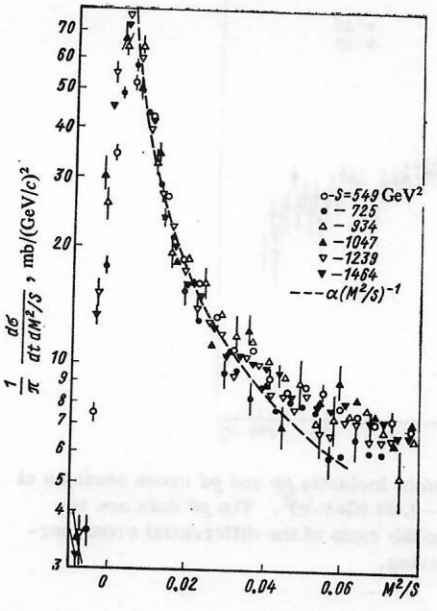

FIG. 18. Dependence of the invariant inelastic cross section of pp scattering on M_X^2/S and S at $t=-0.25$ (GeV/c)^2.

A similar picture is also observed at the higher energies in the measurements made on the colliding beams at CERN at $s=2800$ GeV^2 and $|t|=0.22$ (GeV/c)^2 (Fig. 20).[50] For comparison with pp, the pd cross sections were reduced in proportion to the ratio of the differential cross sections for elastic scattering. In the range of missing masses up to $M_X^2=360$ GeV^2, the pp and pd results agree to within the errors of the measurements.

Turning to the results on the t dependence of the inclusive pp and pd cross sections, we recall that earlier in Fig. 13 we showed an example of the t dependence for the "isobar" $N^*(1400)$.

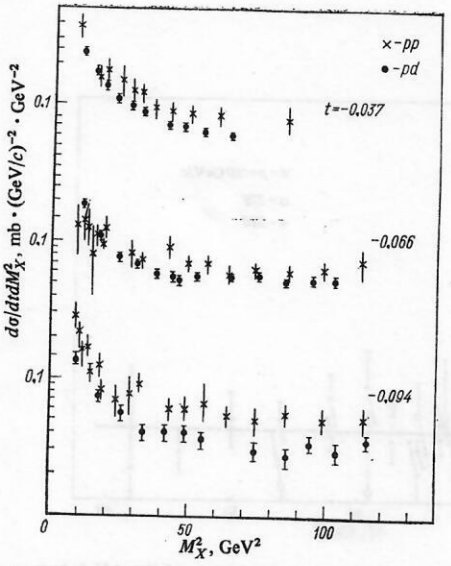

FIG. 19. Comparison of mass spectra for inelastic pp and pd scattering.

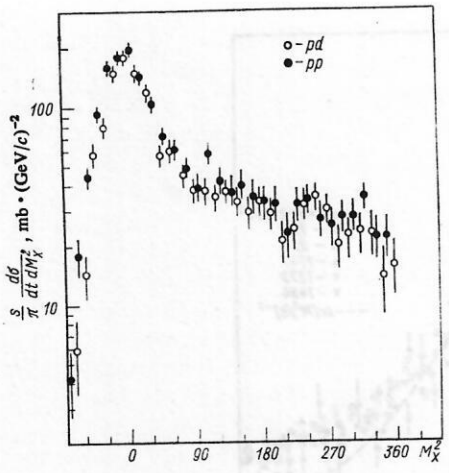

FIG. 20. Comparison of inelastic pp and pd cross sections at $s=2800$ GeV^2 and $t=-0.22$ (GeV/c)^2. The pd data are reduced in proportion to the ratio of the differential cross sections of elastic scattering.

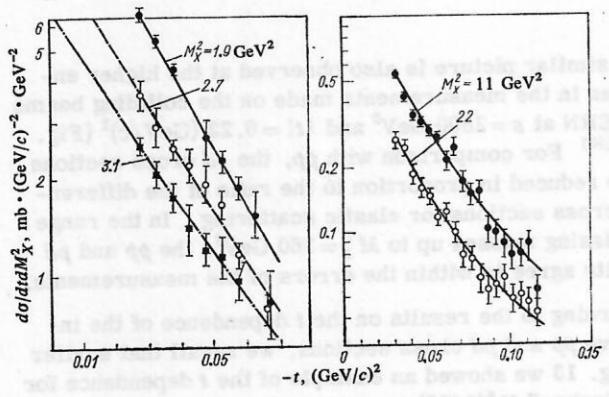

FIG. 21. The t dependence of $d\sigma/dtdM_X^2$ in the reaction $pd \to Xd$ at $p=275$ GeV/c for different missing masses. The curves are the result of fitting in accordance with Eq. (29).

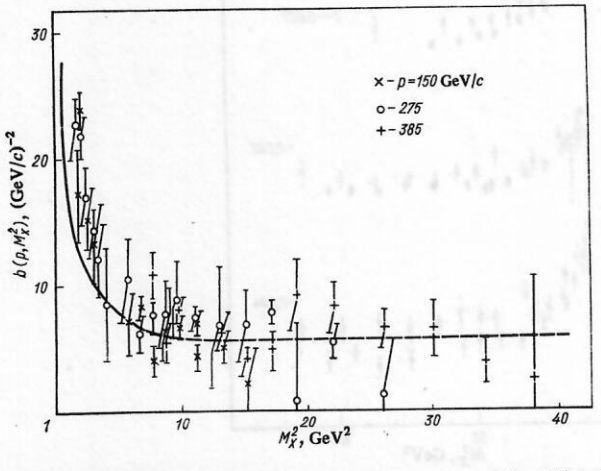

FIG. 22. Dependence of the slope parameter of the pN interaction cross section on M_X^2 and s.

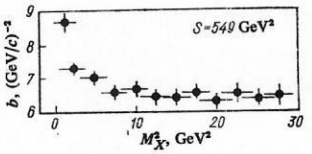

FIG. 23. Slope parameter as a function of M_X^2.

Examples of the t dependences of the differential inclusive pd cross sections for four mass values are given in Fig. 21. In the range $0.02<|t|<0.12$ the differential cross section decreases monotonically with increasing t without exhibiting significant structure.

Assuming nuclear factorization of the pd cross sections, we can readily obtain the value of the slope parameter for nucleon dissociation: $b_N=b_d-b_0$, where $b_0=26.4$ (GeV/c)$^{-2}$ is the slope parameter of the deuteron form factor.

In Fig. 22, we have plotted the dependence of b_N on M_X^2 on the basis of the results taken from Tables II and III. We see that the slope of the diffraction peak has its largest value at $M_X^2\approx 1.9$ GeV^2, where $b_N\approx 24$ (GeV/c)$^{-2}$, then decreases with increasing M_X^2, becoming approximately equal to 6 (GeV/c)$^{-2}$ at $M_X^2\geq 5$ GeV^2 and is then virtually independent of the mass. Note that to within the experimental errors the slope parameter does not depend on the energy.

These features of the behavior of the slope parameter in proton–nucleon inelastic scattering agree well with the new CERN data[41] obtained in the range $0.15<|t|<1.5$ (GeV/c)^2. It is found in Ref. 41 that for $|t|<0.5$

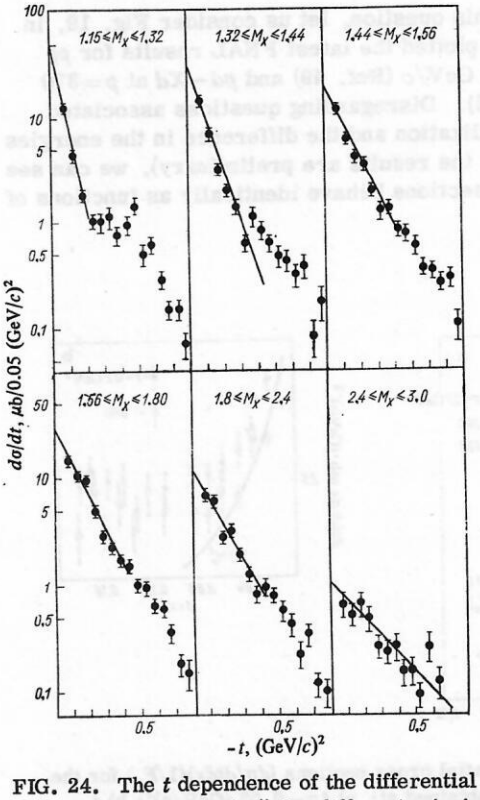

FIG. 24. The t dependence of the differential cross sections of the reaction $pp \to p(n\pi^+)$ for different missing mass intervals.

$(\mathrm{GeV}/c)^2$ the t dependence of the differential cross section can be well described by a simple exponential, and the parameter b is larger at small masses and becomes independent of M_X^2 at large M_X^2. Figure 23 shows the parameter b as a function of M_X^2 as found in this experiment. The somewhat smaller value of the slope parameter at small masses could be explained by the poor mass resolution in this experiment, which was s/M_X^2 times worse than in the experiments with the jet target.

The same circumstance meant that it was not possible in this experiment to see the two slopes in the region of small masses that can be clearly seen in many exclusive experiments.[48, 51] Figure 24 shows the t dependence of the differential cross sections of the reaction $pp \to p(n\pi^+)$ for different missing-mass ranges. One can clearly see the change in the slope parameter at $t \approx 0.2$–$0.4\ (\mathrm{GeV}/c)^2$.

2. THEORETICAL MODELS AND COMPARISON OF THEM WITH EXPERIMENT

Diffraction excitation of hadrons to states with small mass

In this section, we shall discuss the origin of the peaks found at small M_X in the cross section for diffraction dissociation of nucleons.

For the mass spectrum of the dissociation $N \to X$ at small $|t|$ the peak at $M_X \approx 1.4$ GeV is the most characteristic feature. In early papers this peak was attributed to the P_{11} (Roper) resonance found in the partial-wave analysis of πN scattering at $M = 1470$ MeV. However, this interpretation encountered a number of objections.[52]

1. The contribution of the Roper resonance is much less than the contribution of $N^*(1500)$ and $N^*(1688)$, it cannot be seen in the total cross section of πN scattering with isospin $I = \frac{1}{2}$, and it can be distinguished only in a detailed partial-wave analysis. But the peak at $M_X \approx 1.4$ GeV is the dominant structure in the diffraction dissociation cross section at small M_X and $|t|$.

2. In the exclusive channels $N \to \pi N$ and $N \to \pi\pi N$ there is an appreciable shift in the position of the peak maximum (1250 and 1450 MeV, respectively), in contrast to the decay of ordinary resonances into different channels.

3. The total width of the peak in the diffraction dissociation is appreciably greater than the one found by partial-wave analysis for the Roper resonance.

4. In the framework of the resonance model, it is not possible to obtain an explanation for the strong dependence of the slope parameter on the mass of the final system.

Some clarity about the nature of the peak could be achieved by a partial-wave analysis of the basic exclusive channels of diffraction dissociation in the region $M_X \approx 1.4$ GeV. We recall that a similar analysis was successfully used to study the diffraction dissociation processes $\pi \to 3\pi$ and $K \to \pi\pi K$ and revealed that in the majority of cases the phases of the partial-wave amplitudes that are predominant at the peaks do not have a resonance behavior. Unfortunately, a partial-wave analysis of the channel $N \to \pi N$, which is the main one in the region of $M_X \approx 1.4$ GeV, has not yet been made. Recently, data were published[53] of a first analysis of the two-pion channel $pp \to (\pi^+\pi^- p)p$, and these showed that the previously assumed[54, 55] interpretation of the 1470 and 1700 peaks as the resonances $1/2^+(1470)$ and $5/2^+(1688)$ is incorrect. In the region of the first peak, the $3/2^-$ wave and not the dominant $1/2^+$ state has resonance behavior. Below, we shall return to the discussion of the resonance structure of the diffraction dissociation peaks. Here, we merely mention that these facts indicate that not all peaks in the diffraction dissociation mass spectrum can be identified with the excitation of "true" resonances. To see what mechanism can lead to the appearance of peaks in the nonresonance diffraction dissociation amplitudes, we turn to the optical model.

In accordance with Ref. 3, the incident hadron $|\tilde{\lambda}\rangle$ and any state $|\tilde{\lambda}_i\rangle$ to which it can be transformed by the diffraction process can be represented as a superposition of "virtual" or "diffractive" states

$$|\tilde{\lambda}_i\rangle = \sum_k \alpha_{ik} |\lambda_k\rangle. \tag{32}$$

Here, the $|\tilde{\lambda}_k\rangle$ have the same quantum numbers as the original hadron. By hypothesis, the states $|\lambda_k\rangle$ have the following property: They can be absorbed into other (nondiffraction) channels $|\mu_k\rangle$ and as a result of this can be scattered elastically. The amplitude of the diffraction transition from state i to state j is

$$\langle\tilde{\lambda}_j | T | \tilde{\lambda}_i\rangle = (1 - \tilde{\eta}_i)\,\delta_{ij} + \sum_k (\eta_k - \tilde{\eta}_i)\,\alpha_{jk}\alpha_{ki}^{-1}. \tag{33}$$

Here, η_k and $\tilde{\eta}_i$ are the absorption parameters of the diffractive states and the initial (physical) state. The first term in the expression (33) describes the elastic diffraction scattering of physical hadrons, whereas the second describes the diffraction production of particles, i.e., diffraction dissociation. It can be seen that the diffraction dissociation amplitude is proportional to the difference between the absorption amplitudes of the produced system and the incident particle (Fig. 25). Thus, to calculate the diffraction dissociation amplitude in this approach, it is necessary to determine the connection between the real and the diffractive states, and also the elastic scattering amplitude of the diffractive particles. With regard to the choice of the diffractive states, the situation here is very indefinite. They may be real particles, resonances, quarks, partons, etc. In what follows, we shall assume that the main contribution to (32) is made by diffractive states that are close to real particles, i.e., in (32), $\alpha_{ik} = \delta_{ik} + \varepsilon_{ik}$ $(\varepsilon_{ik} \ll 1)$, and to be specific we shall consider the dissociation $N \to \pi N$. Then, ignoring ε^2 and double scattering terms,

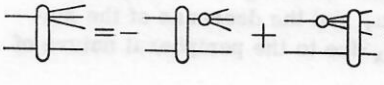

FIG. 25. Amplitude of diffraction production in the optical model.

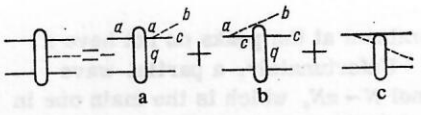

FIG. 26. Diagram for $NN \to \pi NN$ dissociation.

we obtain[52,56] the result shown in Fig. 26.

Note that the diagrams (see Figs. 26b and 26c) have the same vertices and propagators but occur with different signs. Since they contain singularities in different channels, in the general case their contributions are not the same. However, in the (unphysical) limit $t \to 0$ and $M_X^2 \to m^2$ the contributions of the diagrams in Figs. 26b and 26c cancel.[52,57] If it is assumed that this canceling is also important in the physical region of small $|t|$ and M_X, we arrive at a description of the $NN \to \pi NN$ process by means of only the amplitude corresponding to the diagram of Drell and Hiida[58] and Deck[59] (see Fig. 26), which was introduced on the basis of other arguments.

The Drell–Hiida–Deck (DHD) diagram is shown separately in Fig. 27. The lower block contains the amplitude of scattering of a virtual pion on a nucleon, $\tilde{T}_{\pi N}$, and the upper the vertex for emission of a meson and the meson propagator. Since the diffractive particles are by hypothesis close to real particles, the amplitude $\tilde{T}_{\pi N}$ can be replaced by the scattering amplitude $T_{\pi N}$ of a real pion and the πNN vertex by the renormalized pion–nucleon coupling constant. In this case, the amplitude of the diagram in Fig. 27 is completely determined and gives a unique prediction for the $NN \to \pi NN$ diffraction dissociation cross section. However, this naive model does not agree well with the experiments, predicting a too large value of the cross section, broad mass distribution, and small slope of the differential cross section. One can describe the experiments reasonably only by introducing an additional dependence on t_1, which is usually interpreted as allowance for the departure of the pion from the mass shell. By choosing one or two free parameters in this case one can reconcile the required value of the cross section with the shape of $d\sigma/dM$ and the slope parameter. The DHD model has been widely used to describe diffractive dissociation (see, for example, Ref. 60) and successfully explains many characteristic features of diffractive dissociation simply as the result of the corresponding properties of the πN scattering amplitude (weak energy dependence, predominance of vacuum exchange, approximate constancy of the particle and antiparticle cross sections, approximate factorization). In this model, some properties of diffractive dissociation are a consequence of kinematics.

1. The peaks at small masses have a kinematic origin and come about because of two factors: the phase factor, which leads to the vanishing of the amplitude at the threshold $M_X = m + \mu$, and the decrease of the matrix element at large M_X due to the peripheral nature of the collision.[61]

2. The strong dependence of the slope parameter of the differential cross section on the mass M_X can be explained as a consequence of the double peripheral nature of the diagram (see Fig. 27): $T \sim \exp(Bt + B_1 t_1)$. At the threshold ($M_X = m + \mu$), t_1 and t_2 are related linearly, and therefore $T \sim \exp[(B + B_1)t]$. With increasing M_X, the dependence of t_1 on t becomes weaker, leading to a weaker dependence of T on t.

3. The difference in the position of the peaks for the πN and $\pi\pi N$ channels can be naturally explained by the difference between the masses of the final particles.

If it is assumed that at high energies the total cross section of πN scattering does not depend on the energy, then it is possible to integrate explicitly with respect to three of the five independent variables and represent the inclusive cross section $d\sigma/dt dM_X^2$ in the closed form[52]

$$\left(\frac{d\sigma}{dt\, dM_X^2}\right)_0 = \frac{\pi R_1}{4qp_1}\left[\Phi(x_-) - \Phi(x_+)\right], \tag{34}$$

where

$$R_1 = \frac{1}{8\pi^2}\left(\frac{\sigma_{\pi N}}{4\pi}\right)^2\left(\frac{G_{\pi NN}}{s}\right)^2 \frac{q}{M_X}\exp\left[(b_{\pi N} + \delta')\, t\right];\quad \Phi(x)$$
$$= \exp(\delta x)\left(\frac{\gamma}{\delta}x - \frac{\gamma}{\delta^2} + \frac{\beta + \mu^2\gamma}{\delta} - \frac{\mu^2\alpha}{x}\right) + \mathrm{Ei}(\delta x)\,(\alpha + \mu^2\beta + \mu^2\alpha\delta);$$

$\mathrm{Ei}(x)$ is the exponential integral; $x_\pm = a - \mu^2 \pm b$, and a, b, α, β, γ are kinematic quantities determined in Ref. 52; δ and δ' are two free parameters that take into account the departure from the mass shell in the upper and lower blocks of the diagram in Fig. 27. For the amplitude of elastic πN scattering, the following parametrization is used:

$$f_{\pi N} = i\sigma_{\pi N}\exp(bt/2). \tag{35}$$

The experimental data[12,16] are compared with calculations[52] in accordance with Eq. (34) with allowance for the transitions $p \to \pi^0 + p$ and $p \to n + \pi^+$ in Figs. 11 and 22.

The assumption that $\sigma_{\pi N}$ does not depend on the energy corresponds to allowance in the πN scattering amplitude for only the contribution of the pomeron pole P. In the general case, with allowance for secondary trajectories ($R = f, \rho$) we have

$$T(\pi^\pm p \to \pi^\pm p) = T_P + T_f \pm T_\rho;$$
$$T(\pi^0 p \to \pi^0 p) = T_P + T_f, \tag{36}$$

where $T_i = \beta_i(t) X_i(t) s_1^{\alpha_i(t)-1}$; $\alpha_i(t)$ and $\beta_i(t)$ are the trajectory and residue of pole i; $X_i(t)$ is the signature factor

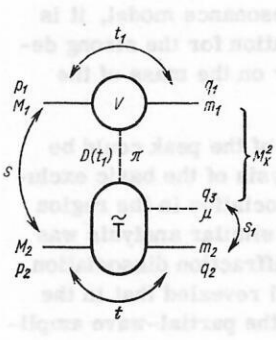

FIG. 27. Diagram of Drell–Hiida–Deck type.

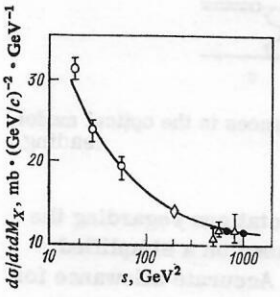

FIG. 28. Energy dependence of the cross section of diffraction dissociation of nucleons at $t = -0.04$ GeV^2 and $M_X = 1.4$ GeV.

$$X_i(t) = -[1+\tau_i \exp(-i\pi\alpha_i)]/\sin\pi\alpha_i; \quad (37)$$

s_1 is the energy of the πN system (see Fig. 27), and it is related to s by

$$s_1 = A(s) + B(s)\cos\theta + C(s)\sin\theta\cos\varphi. \quad (38)$$

Here, A, B, and C are known functions of s and M_X^2 (Ref. 52); θ and φ are the polar and azimuthal emission angles of the nucleon with momentum q_1 (see Fig. 27).

Ignoring the small contribution of ρ exchange, we can write the inclusive cross section in the form

$$\frac{d\sigma}{dt\,dM_X^2} = \int_{-1}^{+1} d\cos\theta \int_0^{2\pi} d\varphi\varphi(s, t, \theta, \varphi, M_X^2) \exp(b_{\pi N}t)\,\sigma_{\pi N}^2 F_1(s_1, t),$$

where

$$F_1(s_1, t) = \tilde{\beta}_P |X_P|^2 s_1^{2\alpha_P - 2} + 2\tilde{\beta}_P\tilde{\beta}_R \operatorname{Re}[X_P^* X_f]\, s_1^{\alpha_P+\alpha_R-2} + \tilde{\beta}_R^2 |X_f|^2 s_1^{2\alpha_R-2}, \quad (39)$$

$$\tilde{\beta} = \beta_i \exp(-b_{\pi N}t)\,\sigma_{\text{tot}}^{-1}(\pi N).$$

The s_1 dependence introduced by the secondary contributions prevents one from calculating the cross section analytically. However, for estimates we can use a simple approximation for (37). At the threshold[62] ($M_X = m + \mu$), we have $s_1 = s/\lambda$, $\lambda = (m+\mu)/\mu$, and

$$\frac{d\sigma}{dt\,dM_X^2} \approx F(s, t)\left(\frac{d\sigma}{dt\,dM_X^2}\right)_0, \quad (40)$$

where

$$F(s, t) = \sum_{i,j} D_{ij}(t)\, s^{\alpha_i(t)+\alpha_j(t)-2};\ i, j = P, R; \quad (41)$$

$$D_{ij} = (\lambda)^{2-\alpha_i(t)-\alpha_j(t)}\,\tilde{\beta}_i(t)\,\tilde{\beta}_j(t)\operatorname{Re}(X_i^*(t)\,X_j(t)). \quad (42)$$

For the $\tilde{\beta}_P$ and $\tilde{\beta}_R$ values found from the πN scattering data and small $|t|$ we have

$$F(s, t) \approx 0.79\exp[(0.5\ln s - 4)t] + 4.2\exp[-5.5t + \ln s(-0.5 + 1.25t)] + 11.1(1 - 3.1t)\exp[-7.1t + (2t-1)\ln s]. \quad (43)$$

The s dependence of the cross section (at $M_X = 1.4$ GeV) calculated in accordance with Eq. (43) agrees well with the experimental data (Fig. 28). We note in passing that a formula of the form $A(M_X^2) + B(M_X^2)s^{-1/2}$ such as was used in earlier papers to extrapolate the mass spectrum to $s \to \infty$ is incorrect since it does not take into account the more complicated s and t dependence associated with the contribution of the secondary trajectories.

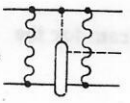

FIG. 29. Drell–Hiida–Deck diagram with absorption.

Let us return to the M_X and t distributions. To obtain the correct absolute value and position of the peak we have had to introduce rather large corrections for the departure of the pion from the mass shell ($\delta = 2$, $\delta' = 3$). However, as can be seen in Fig. 22, even this was insufficient to describe the experimental values of the slope parameter. A way out of this difficulty was indicated in Ref. 52 (see also Ref. 63); it consists of allowing for the absorptive effects associated with the scattering of the particles in the initial and final states (Fig. 29). These effects lead to an important modification of the scattering amplitude.[52]

1. The absolute value of the diffraction dissociation cross section is approximately halved from the prediction of the DHD model (without form factors).

2. Additional t and t_1 dependences appear. Thus, it is no longer necessary to make the unjustified introduction of large off-shell corrections.

3. The slope of the differential cross section in the region of small M_X is increased and the correlation between B and M_X becomes stronger.

4. The differential cross section acquires a minimum for small M_X at $|t| \approx 0.2$–0.3 (GeV/c)^2. Such a minimum was indeed actually discovered recently in experiments at CERN and Batavia.[48, 64]

5. The DHD model with allowance for absorption naturally explains the experimentally found increase in the violation of the s-channel helicity with increasing mass M_X of the system.

6. Just as happens in nondiffraction binary reactions, the absorption suppresses the central contributions and gives a peripheral profile for the diffraction dissociation. Figure 30 shows the $NN \to \pi NN$ diffraction dissociation profile in the region of small masses calculated in the simple DHD model with absorption.[52, 65] As can be seen in Fig. 30, the diffraction transition $N \to \pi N$ takes place basically on the periphery in a "ring" of radius approximately equal to 0.8 F. We shall see below that the peripheral nature found in the region of

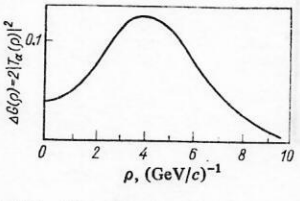

FIG. 30. Amplitude of diffraction dissociation of nucleons in the impact-parameter representation calculated in the simple Drell–Hiida–Deck model with absorption.

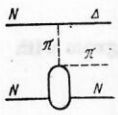

FIG. 31. Drell–Hiida–Deck diagram for the dissociation $NN \to \pi\Delta N$.

small M_X also occurs at large M_X.

Hitherto, we have considered only the region of small M_X, in which the channel $N \to \pi N$ predominates. With increasing M_X, the new channel $N \to \pi\pi N$ is opened, and its contribution can be readily estimated[52] in the framework of the same DHD model by taking into account $\pi\Delta$ production (Fig. 31). One can go further and assume that the $N \to X' + \pi$ DHD mechanism is also responsible for the dissociation in the region $M_X \lesssim 2$–3 GeV. In this case, the inclusive cross section can be expressed in terms of the total cross section of πN scattering[66, 67]:

$$\frac{d\sigma}{dt\,dM_X^2} \approx \frac{\pi}{(2\pi)^6 32 s p_1^2 M_X} \int ds_2 |\mathbf{q}_1| \int d\Omega_1 \operatorname{Im} T_{\pi N}(t_1' = 0) \frac{|T_{\pi N}|^2}{(t_1 - \mu^2)^2}. \quad (44)$$

The results of calculations are shown in Fig. 32. The sum of the two curves gives a peak at $M_X \approx 1.4$ GeV with a shoulder at $M_X \approx 1.7$ GeV, i.e., it reproduces the main features of the mass spectrum of diffraction dissociation at small M_X.

Detailed study of the diffraction dissociation mechanism requires one to use information about the different exclusive channels that contribute to the inclusive cross section. A detailed discussion of the exclusive processes would go beyond the framework of the present review, and we restrict ourselves here to a few comments.

Taking into account the probable canceling, we ignored the contributions of the crossed graphs (see Figs. 26b and 26c). It was noted in Ref. 68 that experiment possibly indicates an important role of these diagrams. One of the arguments relates to the crossover in the reactions $K(\bar{K}) \to Q^0(\bar{Q}^0)$ and $\pi^\pm p \to \pi^\pm(\pi^- \Delta^{++})$, which is simply explained if crossed diagrams with K^* and Δ exchange are taken into account. Another argument is based on the correlation between the decay products of the system excited in the $np \to (\pi^- p)p$ reaction between the polar and azimuthal angles θ and ϕ (Ref. 51), which cannot be explained by just the DHD pion graph. It was conjectured[68] that the peak observed experimentally at $\cos\theta = -1$ and $\phi = 0$ can be explained if nucleon exchange is taken into account (see Fig. 26c). However, as was

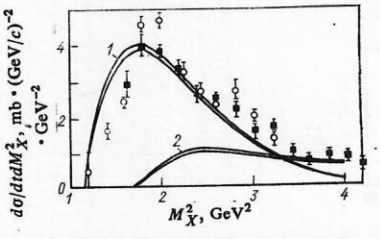

FIG. 32. Mass distribution for the reaction $pp \to Xp$ at $t = -0.027$ (GeV/c)^2 in the model of Drell–Hiida–Deck type: 1) the $N \to \pi N$ contribution; 2) the remaining contributions.

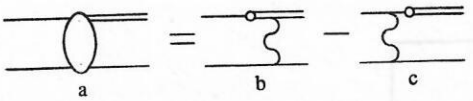

FIG. 33. Direct production of resonances in the optical model.

shown in Ref. 69, the naive expectations regarding the properties of this contribution based on a simplified treatment need not be justified. Accurate allowance for the spin structure of the amplitude under the assumption of conservation of the s-channel helicity in elastic scattering has the consequence that the amplitude (see Fig. 26c) gives a θ/ϕ distribution similar to the DHD pion graph, so that it does not solve the problem.

Note that allowance for the crossed diagrams can lead[70] to a displacement of the DHD peak to larger M_X, which, as can be seen in Fig. 11, leads to better agreement with the experiment.

Note also the following interesting circumstance. When allowance is made on the basis of the model of Ref. 52 for the absorptive corrections to all three diagrams in Fig. 26, there is a cancellation of the absorptive corrections to the crossed terms, and the amplitude can be represented in the form of the pion contribution with absorption and the crossed contributions without absorption.

Above, as diffractive states, we considered only states close to real particles. It is natural to assume that the spectrum of diffractive states is larger and includes, in particular, resonances. A contribution of resonances is rather clearly present in the mass spectrum of diffraction dissociation (see Fig. 15). Besides the production of resonances through the DHD mechanism, which we have already mentioned in connection with the channel $N \to \pi\Delta \to \pi\pi N$ (see Fig. 31), one can also allow direct production (Fig. 33a), which in the framework of the optical model is represented by the diagrams of Figs. 33b and 33c.

A "two-component" model including the contribution of the DHD amplitude and direct production of resonances was first proposed in Ref. 71 to describe photoproduction of ρ mesons. In the two-component model, one has the attractive possibility of reconciling the presence of the resonance contribution to diffractive dissociation with the nonresonance behavior of the phase of the corresponding partial wave, which is very important in connection with the nonresonance behavior of the phases mentioned above for the series of π, K, and N peaks in diffraction dissociation. (Unitarity requires one to allow for not only the DHD and direct production contributions but also the resonance rescattering of particles produced through the DHD mechanism (Fig. 34). In this case, under fairly natural assumptions about the phase of the DHD amplitude, one can have

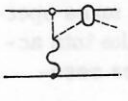

FIG. 34. Pion production through the Drell–Hiida–Deck mechanism with rescattering.

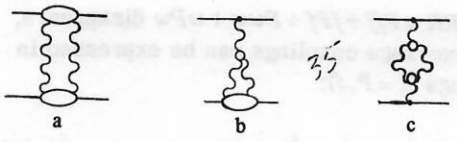

FIG. 35. Contribution of the two-reggeon cut and the diagrams with three-reggeon vertices.

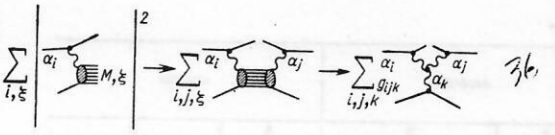

FIG. 36. Inclusive cross section in the three-reggeon formalism.

"compensation" of the resonance behavior of the phase in the total amplitude.)

The two-component model with allowance for absorption can also explain the θ/ϕ correlation.[69] Note that in the two-component model the problem of the shift of the peak at $M_X \approx 1.4$ GeV to larger M_X can be solved by assuming that the contribution of the resonance $N^*(1470)$ is important and that the nonresonance pedestal associated with the DHD mechanism is responsible for only part of the total peak at $M_X \approx 1.4$ GeV.

Summarizing the discussion of the region of small masses, we can say that the main features of diffractive dissociation in this region can be explained on the basis of the DHD model with absorption. The "fine structure" of the main peak in the mass spectrum indicates the presence of resonance contributions, some of which can be attributed to the contributions of resonances produced through the DHD mechanism (of the type shown in Fig. 31). Among the possible resonance candidates—the isobars $N^*(1470)$, $N^*(1500)$, $N^*(1688)$—it is possible that crossed contributions also play an important role in the region of small M_X.[1)]

Excitation of large-mass states

Among the models used to describe diffraction dissociation in the region of large masses M_X, the one that has been developed furthest is the Regge model with allowance for three-reggeon interaction. The concept of three-reggeon interaction arose first in connection with the calculation of the contribution of the cuts that take into account the exchange of several Regge poles (Fig. 35a). If the amplitude of N scattering of reggeons on particles contains a Regge pole, then there exist diagrams of the type shown in Figs. 35b and 35c containing three-reggeon vertices.

The appearance of three-reggeon vertices in the calculation of the diffraction dissociation cross section is shown in Fig. 36. It is assumed that for $s/M_X^2 \gg 1$ the amplitude of the process shown in Fig. 37 can be described by the sum of contributions of Regge poles:

$$T(s, t, M_X^2) = \sum_i \beta_i(t) X_i(t) A(h+\alpha_i \to X) (s/M_X^2)^{\alpha_i(t)}. \tag{45}$$

We can regard $A(h+\alpha_i \to X)$ as the amplitude of transition of the hadron h and the reggeon α_i with mass $\sqrt{-t}$ into the hadronic state X. Squaring Eq. (45) and summing over all possible states of the system X, we obtain the inclusive cross section

$$\frac{d\sigma}{dt\,dM_X^2} = (16\pi s^2)^{-1} \sum_{i,\,j,\,X} \beta_i \beta_j X_i X_j^* A(h+\alpha_i \to X) \times A^*(h+\alpha_j \to X) \left(\frac{s}{M_X^2}\right)^{\alpha_i+\alpha_j}. \tag{46}$$

Let us consider first the diagonal terms ($i=j$) and sum over the states X for fixed M_X:

$$\sum_X |A(h+\alpha_i \to X)|^2 = M_X^2 \sigma_{h\alpha_i}(M_X^2, t), \tag{47}$$

where $\sigma_{h\alpha_i}(M_X^2, t)$ is the total cross section for the interaction of reggeon i and the hadron at cms energy M_X. If M_X is sufficiently large, $\sigma_{h\alpha_i}(M_X^2, t)$ can also be expressed by means of the contributions of Regge poles:

$$\sigma_{h\alpha_i}(M_X^2, t) = \sum_k \beta_k(0) \operatorname{Im} X_k(0)\, g_{iik}(t) (M_X^2)^{\alpha_k(0)-1}, \tag{48}$$

where $g_{ijk}(t)$ is the three-reggeon vertex shown in Fig. 36. Substituting (47) and (48) in (46) and taking into account also the nondiagonal terms, we obtain finally the following expression for the inclusive cross section[72]:

$$\frac{d\sigma}{dt\,dM_X^2} = \sum_{ijk} G_{ijk}(t)\, s^{\alpha_i(t)+\alpha_j(t)-2} (M_X^2)^{\alpha_k(0)-\alpha_i(t)-\alpha_j(t)}, \tag{49}$$

where

$$G_{ijk}(t) = (16\pi)^{-1} \beta_i(t) \beta_j(t) X_i(t) X_j^*(t) \operatorname{Im} X_k(0) \beta_k(0) g_{ijk}(t).$$

Besides the variables M_X^2 and t, it is convenient to use the variables x and p_T. If $M_X^2/s \ll 1$, we have $x = 2p_\parallel/\sqrt{s} \approx 1 - M_X^2/s$ and $t \approx -p_T^2$. The dependence on s, M_X^2, and x of the various contributions to the cross section (2.18) is given in Table V for $\alpha_P(t) = 1+\gamma t$, $\alpha_R(t) = \frac{1}{2} + \beta t$, and $\alpha_\pi(t) = \delta t$.

As can be seen from Table V, in the case when contributions with only $k=P$ are important at large M_X, the cross section depends only on the variable x, i.e., we have scaling. In particular, the contribution of the three-pomeron interaction leads to the dependence

$$d\sigma/dt\,dM_X^2 = G_{PPP}(t) (s/M_X^2)^{2\alpha_P(t)-2} (M_X^2)^{\alpha_P(0)}. \tag{50}$$

Bearing in mind that the cross section of elastic pp scattering in the Regge pole model is

$$s^2 \left(\frac{d\sigma}{dt}\right)_{pp} = \frac{1}{16\pi} \left| \sum_i \beta_i^2(t) X_i(t)\, s^{\alpha_i(t)} \right|^2,$$

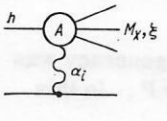

FIG. 37. Dissociation amplitude in the Regge model.

[1)] Note however that inclusion of crossed terms and resonances may result in a contribution being taken into account twice.

TABLE V.

Three-reggeon terms	$d\sigma/dtdM^2$		$d\sigma/dtdx$	
ijk	A	B	A	B
PPP	$1/M^2$	$\frac{s^{2\gamma t}}{(M^2)^{1+2\gamma t}}$	$1/(1-x)$	$\frac{1}{(1-x)^{1+2\gamma t}}$
PRP	$1/(M\sqrt{s})$	$\frac{s^{\alpha_0+(\beta+\gamma)t-1}}{(M^2)^{\alpha_0+(\beta+\gamma)t}}$	$1/(1-x)^{1/2}$	$\frac{1}{(1-x)^{\alpha_0+(\beta+\gamma)t}}$
RRP	$1/s$	$\frac{s^{2\alpha_0+2\beta t-2}}{(M^2)^{2\alpha_0+2\beta t-1}}$	1	$\frac{1}{(1-x)^{2\alpha_0+2\beta t-1}}$
PPR	$1/M^3$	$\frac{s^{2\gamma t}}{(M^2)^{2-\alpha_0+2\gamma t}}$	$1/\sqrt{s}\times$ $\times 1/(1-x)^{3/2}$	$\frac{(M^2)^{\alpha_0-1/2}}{\sqrt{s}\,(1-x)^{3/2+2\gamma t}}$
PRR	$1/(M^2\sqrt{s})$	$\frac{s^{\alpha_0+(\beta+\gamma)t-1}}{(M^2)^{1+(\beta+\gamma)t}}$	$1/\sqrt{s}\times$ $\times 1/(1-x)$	$\frac{1}{s^{1-\alpha_0}(1-x)^{1+(\beta+\gamma)t}}$
RRR	$1/(sM)$	$\frac{s^{2\alpha_0+2\beta t-2}}{(M^2)^{\alpha_0+2\beta t}}$	$1/\sqrt{s}\times$ $\times 1/(1-x)^{1/2}$	$\frac{1}{s^{1-\alpha_0}(1-x)^{\alpha_0+2\beta t}}$
$\pi\pi P$	M^2/s^2	$\frac{s^{2\delta t-2}}{(M^2)^{2\delta t-1}}$	$(1-x)$	$\frac{1}{(1-x)^{2\delta t-1}}$
$\pi\pi R$	M/s^2	$\frac{s^{2\delta t-2}}{(M^2)^{2\delta t-\alpha_0}}$	$1/\sqrt{s}\times$ $\times(1-x)^{1/2}$	$\frac{1}{\sqrt{s}\,(1-x)^{2\delta t-\alpha_0}}$

Note. A are approximate expressions for $\gamma=\beta=\sigma=0$, $\alpha_0=\frac{1}{2}$; B are the total expressions.

we can write down an expression for the pomeron–proton interaction cross section $\sigma_{Pp}(M_X^2, t)$:

$$\sigma_{Pp}(M_X^2, t)=4\sqrt{\pi}\,|X_P(t)|^{-1}\,s^{\alpha_P(t)-1}\left(\frac{d\sigma}{dt}\right)_{pp}^{-1}\times\left[G_{PPP}(t)+\frac{G_{PPR}(t)}{(M_X^2)^{1-\alpha_R(0)}}\right]. \quad (51)$$

Let us now, following Ref. 62, consider in more detail the different exchanges that contribute to (49) in the case of dissociation of nucleons on nucleons. The leading Regge poles coupled to nucleons are P, f, ω, ρ, A_2, and π. The isospin and G parity selection rules reduce the number of possible triple vertices.

1. In PPR and PRP, only PPf and PfP are allowed.

2. In RRP, only ffP, $\omega\omega P$, $\rho\rho P$, A_2A_2P, $\pi\pi P$, and $A_2\pi P$ are possible. If ρ and A_2, which are weakly coupled to the nucleon, are ignored, we obtain ffP, $\omega\omega P$, $\pi\pi P$ for RRP and Pff, fPf, $P\omega\omega$, $\omega P\omega$ for PRR. The $P\pi\pi$ term disappears because of the spin and parity selection rule and the condition that $t=0$ on the k-th leg of the three-reggeon diagram.

3. For RRR in the general case there is a large number of combinations, and we therefore directly ignore the ρ and A_2 contributions. The $f\pi\pi$ and $\pi f\pi$ terms are again eliminated by the spin and parity selection rules, and the $f\omega\omega+\omega f\omega$ term by the exchange degeneracy. The isospin and G parity selection rules allow only fff, $\omega\omega f$, and $\pi\pi f$. One could go further and assume degeneracy of all triple couplings including ω and f trajectories. However, this strong form of exchange degeneracy, which leads to the cancellation of all nondiagonal terms, is false in the general case, [73] since the ωPP and $P\omega P$ terms, which "partner" the fPP and PfP terms, themselves disappear because of the G parity selection rule.

A different, weaker form of exchange degeneracy was proposed in Ref. 74 for only terms with $k\neq P$. In this case, the term $PRR=Pff+fPf+P\omega\omega+\omega P\omega$ disappears, and the other ω-exchange couplings can be expressed in terms of f couplings ($i=P,f$):

$$G_{ffi}+G_{\omega\omega i}=\beta_f^2(t)\,\beta_i(0)\,g_{ffi}(t)\,\frac{4}{\sin^2\pi\alpha_f(t)}.$$

Arguments for this weak form of exchange degeneracy are based on the assumption of normal two-component duality for the nondiffraction terms in (49). However, as we shall see below, this assumption may be false.

Thus, in the general case it is necessary to take into account all six functions G_{ijk} associated with the exchange of the pomeron and the vector and tensor poles (these last are described by the effective pole R), and also the two pion terms. Using the proximity of the pion pole to the physical region, we can[75] express $G_{\pi\pi i}$ directly in terms of the πN interaction total cross section:

$$G_{\pi\pi i}(t)=-\frac{1}{4\pi}\,\frac{g_{\pi NN}^2}{4\pi}\,\sigma_{\text{tot}}^i(\pi p)\,\frac{t\exp[b_\pi(t-\mu^2)]}{(t-\mu^2)^2}. \quad (52)$$

Here, $i=P$ or R; σ_{tot}^P and σ_{tot}^R are the diffraction and nondiffraction contributions to the total πN scattering cross section. The factor $\exp[b_\pi(t-\mu^2)]$ takes into account possible off-shell effects.

As can be seen from Eq. (49), the three-reggeon model makes it possible to parametrize simply the dependence of the cross section on M_X^2, s, and t and serves as a convenient basis for the phenomenological analysis of the experimental data. In the general case, the expression (49) contains a large number of free parameters, for whose finding we must employ experimental data in the widest possible range of the kinematic variables.

Additional restrictions on the three-reggeon vertices can be obtained by means of the duality hypothesis. It is well known that this hypothesis has proved very fruitful in the study of binary reactions. Its mathematical expression takes the form of finite-energy sum rules[76–79] that relate the behavior of the scattering amplitude at low and high energies. A natural generalization of these sum rules for the amplitudes of scattering of reggeons on particles lead to finite-mass sum rules[80–82]:

$$\int_0^{\nu_0}d\nu\nu^n\left\{\frac{d\sigma}{dt\,dM_X^2}(ab\to cX)+(-1)^{n+1}\frac{d\sigma}{dt\,dM_X^2}(cb\to aX)\right\}=\sum_{ijk}G_{ijk}(t)\,\frac{s^{\alpha_i(t)+\alpha_j(t)-2}\,\nu_0^{\alpha_k(0)+n+1-\alpha_i(t)-\alpha_j(t)}}{\alpha_k(0)+n+1-\alpha_i(t)-\alpha_j(t)}, \quad (53)$$

which relate the behavior of the inclusive cross sections at small M_X to the three-reggeon asymptotic behavior (49). In (53), $\nu=M_X^2-t-m^2$ is the cross-symmetric variable. Calculating the left-hand side by means of the experimental data on diffraction dissociation in the region of small M_X, we can use the relation (53) as an additional condition when finding G_{ijk}. Another possibility is to verify the relation (53) and, therefore, the assumptions made in its derivation.

Note that if in the cross section for the excitation of small M_X it were possible to separate the contributions of the individual α_i and α_j exchanges, the relation (53) could be "decoupled" in accordance with the s dependences of the different terms. Unfortunately, this can be done at present only by means of a model. In Ref. 62, it was assumed that: a) semilocal duality holds, i.e., the finite-mass sum rules are true with low cutoff ν_0; b) the entire peak at $M_X \approx 1.4$ GeV is described by the DHD model for $N \to \pi N$; c) the contribution of resonances is negligibly small. The two last assumptions are justified only for small $|t| \lesssim 0.1$ (GeV/c)^2, where the peak at $M_X \approx 1.4$ GeV is predominant. Thus, in this model the left-hand side of (53) is determined solely by the contribution of the elastic scattering (equivalent to the resonance contribution to the finite-energy sum rules) and the DHD contribution (equivalent to the nonresonance background), and Eq. (53) with $n=1$ leads to the relations

$$\begin{aligned} &\langle E_{ij}\rangle + \langle D_{ij}\rangle = G_{ijP} f_{ijP} + G_{ijR} f_{ijR};\\ &f_{ijk} = \nu^{\alpha_k(0)+2-\alpha_i(t)-\alpha_j(t)}/[\alpha_k(0)+2-\alpha_i(t)-\alpha_j(t)]\\ &(i=j=P;\ i=P;\ j=R;\ i=j=R), \end{aligned} \tag{54}$$

which are shown graphically in Fig. 38. In Eq. (54), $\langle E_{ij}\rangle$ and $\langle D_{ij}\rangle$ are the integrals with respect to M_X of the terms corresponding to α_i and α_j exchange in the elastic and DHD amplitudes. As is shown in Ref. 62,

$$\begin{aligned} &\langle E_{ij}\rangle = -tE_{ij};\\ &\langle D_{ij}\rangle = D_{ij} Q(t), \end{aligned} \tag{55}$$

where

$$Q(t) = \int_{\nu_{th}}^{\nu_0} \nu\, d\nu\, (d\sigma/dt\, dM_X^2)_0, \tag{56}$$

and

$$\begin{aligned} &E_{PP} = (16\pi)^{-1} \beta_P^4(t) |X_P(t)|^2;\ E_{RR} = (16\pi)^{-1} 4\beta_R^4(t) \sin^{-2}\pi\alpha_R(t)\\ &E_{PR} = (16\pi)^{-1} 4\beta_P^2(t) \beta_R^2(t) \operatorname{Re} X_P(t) \sin^{-1}\pi\alpha_R(t). \end{aligned} \tag{57}$$

Note that in this approach, in contrast to the one proposed in Ref. 66, the DHD model is used only in the region in which there are gounds for believing it, i.e., in the region of small M_X, and the connection to large M_X is made on the basis of analytic properties taken into account by the finite-mass sum rule.

Further information can be obtained if we can in some way separate the P and R contributions in (54). For ordinary two-particle hadron reactions such a separation, based on the Harari–Freund two-component duality, [83,84] is completely justified. In this case, the contribution of the resonances is related through the finite-energy sum rules to the "ordinary" Regge poles R, while the background is related to the pomeron P. However, this "normal" two-component duality cannot be generalized to the many-particle amplitudes in a direct model-independent manner. [85] Usually, it is assumed that for nonpomeron exchanges, i.e., for the $R+h \to R+h$ and $R+h \to P+h$ amplitudes (h is a hadron), normal two-component duality holds. [86] For the $P+h \to P+h$ amplitude, arguments were put forward in favor of abnormal duality, in which the resonances in the direct channel construct a pomeron in the cross channel. [87] The term abnormal is here used for the extreme case when the entire contribution of the resonances is associated with P, whereas the background constructs R. We shall here distinguish it from the weaker form of mixed duality in which the resonances and background contribute partly to P and partly to R. It should be noted that the secondary vacuum trajectory f can also share with P its abnormal properties. [88] Thus, we shall consider the relations (54) for different types of duality.

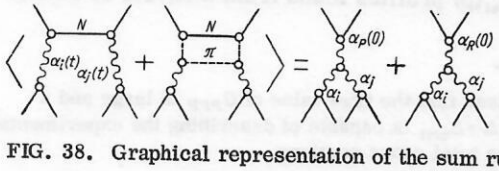

FIG. 38. Graphical representation of the sum rule (54).

In the case of normal two-component duality, Eq. (54) can be decoupled and the following expressions obtained for the three-reggeon vertices:

$$G_{ijP} = \langle D_{ij}\rangle f_{ijP}^{-1};\ G_{ijR} = \langle E_{ij}\rangle f_{ijR}^{-1}. \tag{58}$$

In the case of abnormal duality, it is necessary to make the substitution $E_{ij} \rightleftarrows D_{ij}$ in these expressions. One can also consider the case of mixed duality, for example

$$\begin{aligned} &G_{PPP}(t) = [\varepsilon_1 \langle E_{PP}\rangle + \varepsilon_2 \langle D_{PP}\rangle] f_{PPP}^{-1};\\ &G_{PPR}(t) = [(1-\varepsilon_1)\langle E_{PP}\rangle + (1-\varepsilon_2)\langle D_{PP}\rangle] f_{PPR}^{-1}. \end{aligned} \tag{59}$$

These relations will be analyzed and compared with the experiments below.

Determination of the three-reggeon vertices from analysis of the experimental data on the diffraction dissociation spectra is of particular interest for the theory of strong interactions. A particularly important characteristic is the three-pomeron vertex G_{PPP}, which plays the role of a fundamental constant in asymptotic Regge theory. Depending on its behavior in the limit $t \to 0$, different regimes are obtained at asymptotically high energies.

We consider first of all the case $\alpha_P(0)=1$ and $G_{PPP}(0) \neq 0$. In the simple pole model without allowance for rescattering, the three-pomeron contribution to the total cross section is

$$\sigma_{PPP} \sim \frac{G_{PPP}(0)}{\alpha_P'(0)} \ln\left[\frac{a+2\alpha_P'(0)\ln(s/m^2)}{a-2\alpha_P'(0)\ln(1-x_0)}\right], \tag{60}$$

where a is determined by the proton radius; x_0 is the lower limit of the interval in which the three-pomeron asymptotic behavior is important. In this case, we arrive at a well-known contradiction since the condition $\alpha_P(0)=1$ entails $\sigma_{tot}(s\to\infty) = \text{const}$, whereas the three-reggeon contribution (60) to σ_{tot} increases with the energy.

For $G_{PPP}(0) \neq 0$, if the theory is to be self-consistent, it is necessary to assume that the intercept of the bare

pomeron satisfies $\alpha_P(0) = 1 - \varepsilon < 1$. The parameter $\eta = g_{PPP}^2(0)/32\pi\alpha'_P(0)$, which characterizes the corrections due to the three-pomeron interaction, must be small,[89] so that perturbation theory can be used at the achievable energies. In this case, at small s, the cross section decreases with increasing s because $\alpha_P(0) < 1$, and the growth of the cross section observed at $s \approx 10^2 - 10^3$ GeV^2 is due to the peripheral thresholds resulting from the production of large-mass particles.[90, 91]

If $\alpha_P(0) = 1$, it is necessary[92] to set $G_{PPP}(0) = 0$. If $G_{PPP}(t) \sim |t| \exp(Bt)$, the three-pomeron contribution to the total cross section is

$$\sigma_{PPP} \sim \frac{\ln s(1-x_0)/M_0^2}{B + 2\alpha'_P(0) \ln s/M_0^2} \quad (M_0^2 \approx 4-5 \text{ GeV}^2) \tag{61}$$

and at high energies tends to a constant limit. At the same time, the differential cross sections of all the inelastic processes must vanish as $t \to 0$ and the total interaction cross sections of all particles must be asymptotically equal.[93]

The fairly rapid growth of the total interaction cross sections of hadrons discovered with the Serpukhov, Batavia, and CERN accelerators and also in cosmic rays stimulated interest in models with $\alpha_P(0) = 1 + \Delta > 1$. For example, it was shown in Refs. 94 and 95 that if the intercept of the bare pomeron is equal to $1 + \Delta_{\text{crit}}$, where

$$\Delta_{\text{crit}} = \eta \ln(1/\eta), \tag{62}$$

then there exists a self-consistent solution satisfying both t-channel and s-channel unitarity for which the physical pomeron has $\tilde{\alpha}_P(0) = 1$. However, the existing estimates of the three-pomeron vertex obtained by analyzing the diffraction dissociation spectra lead to a small value of g_{PPP} and accordingly of Δ_{crit} ($\sim 10^{-2}$) and do not describe the experimental growth of the total cross sections. In this connection, models with $\Delta > \Delta_{\text{crit}}$ are of interest.[96-98] In these schemes, at high energies, the contribution of the Pomeranchuk pole to the scattering amplitude increases as $(s/s_0)^{\Delta}$. However, the alternation of sign in the series, which takes into account branch points, restores unitarity and leads to the behavior $\sigma_{\text{tot}} \sim \ln^2(s/s_0)$. The effective singularity corresponding to such behavior is shifted at $t = 0$ to $j = 1$ and is represented by a pair of complex-conjugate branch points. Physically, this corresponds to scattering on a disk with radius that increases as $\ln s$. Thus, in the framework of Regge theory we obtain a picture of the scattering very close to geometrical models of diffraction scattering. At comparatively low energies, the corrections for reggeon interaction are unimportant, and the amplitude can be described by the diffractive pole with $\alpha_P(0) = 1 + \Delta$.

Our discussion above of the various variants of the theory was based on a number of simplifying assumptions, in particular, the use of asymptotic expressions that apply only at superhigh energies and also the pole asymptotic behavior.

The real situation may be considerably more complicated. First of all, arguments against the model with $\alpha_P(0) = 1$ based on comparison of data on the growth of the total cross sections may in reality have no bearing on the matter. As was noted in Ref. 99, in the region of energies currently reached with accelerators, allowance for energy and momentum conservation may lead to a radical change of the asymptotic regime. From this point of view, the region of accelerator energies is a threshold region, and many conclusions based on asymptotic expressions must be reviewed. In particular, the growth of the total cross sections can be explained even with $\alpha_P(0) = 1$.

The second remark applies to the absorptive corrections to the pole exchanges, which, as we have seen above, significantly modify the diffraction dissociation amplitude in the region of small masses. Such a phenomenon also seems to occur at large M_X, the calculations made in Ref. 100 show that the absorption in the three-pomeron region is very important and sensitive to the value of the B'_k slope, which corresponds to the k-th leg of the three-reggeon vertex (see Fig. 36). As a result of allowance for absorption, $d\sigma/dtdM_X^2$ is reduced by a factor 2–4. Therefore, to reproduce the experimental data on the inclusive spectrum, it is necessary to take the three-pomeron vertices greater than their values found in accordance with Eq. (48) from the experiments.[2)] At the same time, since B'_k is not determined experimentally, the exact three-reggeon vertex cannot be extracted from the data. The situation is also aggravated by the fact that the experimental ("effective") vertex obtained from the inclusive data cannot be used in theoretical calculations of, for example, the elastic amplitude since the absorptive corrections to the elastic scattering are different from (much smaller than) those in diffraction dissociation.

An interesting remark was made in Ref. 100 to the effect that, despite the strong absorptive effects, factorization may hold in diffraction dissociation with good accuracy. This indicates, not predominance of pole exchange, but approximate equality of the absorptive corrections in different reactions.

It is to be expected that, as for small M_X, absorption leads to a peripheral profile in the diffraction dissociation in the region of large masses. And, indeed, the analysis made in Ref. 101 under the assumption that the t-channel helicity is conserved in diffraction dissociation led to a peripheral profile for diffraction dissociation of nucleons. An analogous result can also be obtained by means of the bounds[102]

$$\frac{1}{\pi}\frac{d\sigma_{\text{diff}}}{d\rho^2} \leqslant \frac{1}{2\pi}\frac{d\sigma_{\text{tot}}}{d\rho^2} - \frac{1}{\pi}\frac{d\sigma_{\text{el}}}{d\rho^2} \equiv \sigma_{\text{diff}}^{\max}(\rho), \tag{63}$$

deduced from s-channel unitarity under the assumption that elastic and inelastic diffraction constitute the "shadow" of nondiffraction processes. Substituting the $\sigma_{\text{tot}}(\rho)$ and $\sigma_{\text{el}}(\rho)$ profiles found from analysis of elastic

[2)] This may mean that the true value of G_{PPP} is large and a theory with $\Delta = \Delta_{\text{crit}}$ is capable of describing the experimental growth of the total cross sections.

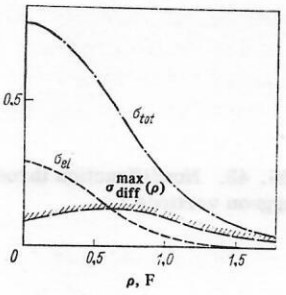

FIG. 39. Distribution with respect to impact parameters of the various contributions to the pp interaction cross section at $\sqrt{s} = 53$ GeV.

scattering into (63), we obtain the boundary $\sigma_{diff}^{max}(\rho)$ shown in Fig. 39 (Ref. 103).

The peripheral nature of the diffraction dissociation contributions can lead to a distinctive phenomenon—small-scale oscillatory structure in the differential cross section of elastic scattering.[65,104] This phenomenon, which was discussed earlier in Ref. 105, was discovered recently[106] in pp scattering and in the scattering of relativistic nuclei.[107]

We now give some results of the analysis of the experimental data based on the three-reggeon formalism and the finite-mass sum rules. We begin with the simple variant of Ref. 108, in which Akimov *et al.* analyze only data obtained for deuterium[16,17] and restrict themselves to a few three-reggeon vertices.

Using the fitting (49) and taking into account the PPP, RRR, and PPR vertices, they found $G_{PPP} = (3.20 \pm 0.36) \times \exp(bt)$, $G_{RRR} = (74 \pm 30) \exp(bt)$, $G_{PPR} = (1.00 \pm 0.63) \times \exp(bt)$ ($\chi^2 = 34.6$ with 28 degrees of freedom). The parameters α_R' and b were fixed at the values 1 and 5 $(\text{GeV}/c)^{-2}$.

With allowance in the framework of these assumptions for the restrictions associated with the finite-mass sum rules, the values of the vertices were changed somewhat: $G_{PPP}(0) = 2.9 \pm 0.25$, $G_{RRR}(0) = 122 \pm 15$, $G_{PPR}(0) = 1.00 \pm 0.14$.

Comparing these values with the extrapolation to $t \approx 0$ of the results of earlier analyses (see the references in Refs. 4–11) based on the data for large $|t|$, we can conclude that in the earlier analyses the purely diffraction PPP coupling at small $|t|$ was underestimated, largely through the overestimation of the role of the PPR term. As we shall see below, a more detailed analysis confirms this conclusion. (At the same time, as was to be expected, allowance for the secondary contributions reduces the value of $G_{PPP}(0)$ compared with the upper limit $G_{PPP}(0) \approx 4.5$ $\mu\text{b} \cdot \text{GeV}^{-2}$ determined in Ref. 15.)

The critical role of the data of Refs. 14 and 17 for understanding the importance of the PPP coupling at small $|t|$ was made very clear in Ref. 109, which makes it possible to follow the evolution in the ratio $G_{PPP}(t)/G_{PPR}(t)$ on the transition from large to small $|t|$. In Ref. 109, Azkarate studied the possibility of describing the $pp \to Xp$ and $pd \to Xd$ data with allowance for the finite-mass sum rules and the PPP and PPR terms under the assumption of f/P universality,[110,111] i.e., under the condition $G_{PPR}(t) = rG_{PPP}(t)$. He found that for $|t| > 0.15$ GeV^2 the data can be well described for $r \approx 1$, although on the transition to small $|t|$ the value of r decreases, i.e., the PPP term predominates. Let us now turn to a discussion of the results of a detailed analysis that takes into account many experimental data and a more complete set of three-reggeon terms.

In Ref. 112, Field and Fox included in their analysis all the then existing data on the $pp \to Xp$ reaction and the finite-mass sum rules and they took into account the PPP, RRR, PPR, RRP, $\pi\pi P$, and $\pi\pi R$ terms. The parameters found by them enable one to calculate the differential cross section and continue it to $t \approx 0$. The result is shown in Fig. 40 for $G_{PPP}(0) \neq 0$ and $G_{PPP}(0) = 0$. Comparison of these curves with the data of Refs. 14 and 17 for small $|t|$ (see Fig. 21b) enables one to draw important conclusions: The assumption that the three-pomeron (effective) vertex vanishes does not agree with the experimental data. (The elimination of the pion terms, which determine basically the difference between exchanges on p and d, does not change this conclusion.)

In this connection we should like to make the following remark. In Ref. 113 it is asserted that the experimental data in a wide range of energies indicate that the effective $G_{PPP}(0) = 0$. However, the solution found in Ref. 113 is unsatisfactory from the physical point of view since it leads in the considered kinematic region to negative values of the diagonal terms ($i = R$, P) in the limit $t \to 0$:

$$\left(\frac{s\,d\sigma}{dt\,dM_X^2}\right)_{ii} = \sum_k G_{iik}(t)\,\frac{(1-x)^{\alpha_k(0)-2\alpha_i(t)}}{s^{1-\alpha_i(0)}}, \qquad (64)$$

which are the product of two complex-conjugate amplitudes associated with the total cross sections $\sigma_{p\alpha_i}(M_X^2)$, and they must be positive definite. The important role of the nondiagonal terms was demonstrated in Ref. 62. These terms were taken into account in Ref. 114 and led to values of the vertices somewhat different from those in Ref. 112. We point out in particular that instead of the value 2.63 mb · $(\text{GeV}/c)^{-2}$ found in Ref. 112 for $G_{PPP}(0)$ the larger value (3.24 ± 0.35) mb · $(\text{GeV}/c)^{-2}$ was obtained.

In the papers discussed above, it was assumed that $\alpha_P(0) = 1$. In Ref. 115, Chu *et al.*, also discussed the model with $\alpha_P(0) = 1 + \Delta$, which has recently been often discussed. The paper Ref. 115 is also interesting in that it included the data of Refs. 14 and 17 at small $|t|$

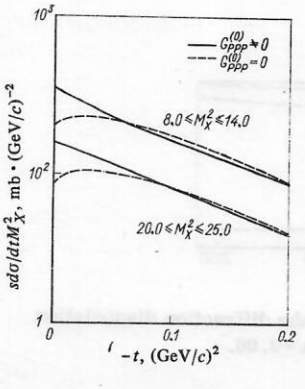

FIG. 40. The cross section $sd\sigma/dtdM_X^2$ calculated in Ref. 112 at $p = 400$ GeV/c.

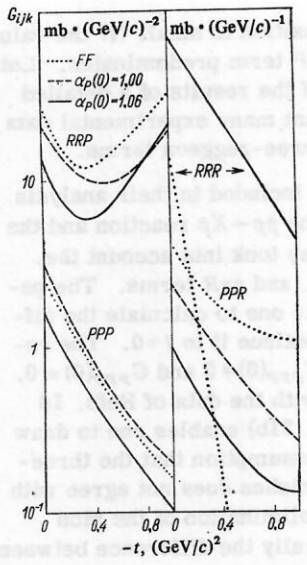

FIG. 41. Three-reggeon vertices[112] for $\alpha_p(0)=1$, $\alpha_p(0)=1.06$.

and eliminated the erroneous data of Refs. 36 and 37. As in Ref. 112, the PPP, RRR, PPR, RRP, $\pi\pi P$, and $\pi\pi R$ terms were taken into account. The values of the vertices found by the fitting are shown in Fig. 41. The most interesting feature in the solution for $\Delta=0$ is the reduction by about a factor two in the value of $G_{PPP}(0)$ compared with Ref. 112. This is due to the elimination of the data of Refs. 36 and 37, which indicated a large term $\sim M^{-3}$, and the inclusion of the data of Refs. 14 and 17, which indicated the importance of the term $\sim M^{-2}$. This last is confirmed by the nearly scaling behavior of $sd\sigma/dtdM_X^2$ at small $|t|$. However, at $t=-0.16$ (GeV/c)^2 the contribution of the PPR term is certainly necessary.

The main difference between the solution with $\Delta\neq 0$ and the solution with $\Delta=0$ is the decrease in G_{PPR} and the increase in G_{RRR}. In addition, G_{PPP} is somewhat decreased. In the calculations, $\Delta=0.06$ was used, which leads to a good description of the growth of $\sigma_{tot}(pp)$. The contribution of inelastic diffraction scattering to the total cross section

$$\sigma_D(s)=\frac{2}{s}\int_2^{0.2s} dM_X^2 \int_{-\infty}^{t_{min}} dt \left\{ G_{PPP}(t)\left(\frac{M_X^2}{s}\right)^{1+\Delta-2\alpha_P(t)} + G_{PPR}(t)\left(\frac{M_X^2}{s}\right)^{0.5-2\alpha_P(t)}\frac{1}{\sqrt{s}}\right\} \quad (65)$$

is shown in Fig. 42. The growth of σ_D as p increases

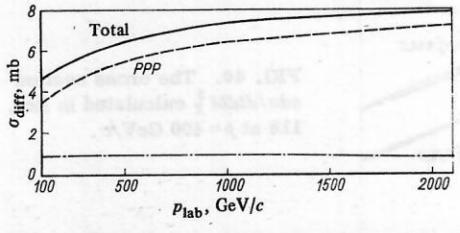

FIG. 42. Energy dependence of the diffraction dissociation cross section in the model with $\Delta=0.06$.

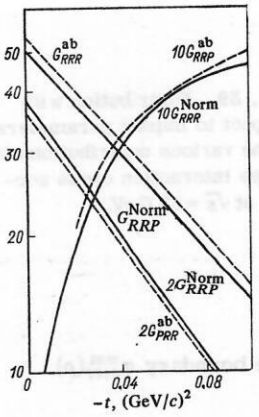

FIG. 43. Nondiffraction three-reggeon vertices.

from 300 to 1500 GeV/c is about 1 mb at $\Delta=0$ and about 2 mb at $\Delta=0.06$. Taking into account the results of Ref. 115, we can draw the following conclusions: a) There is no indication that $G_{PPP}(t)$ vanishes as $t\to 0$; b) there is contraction with $\alpha'_P\approx 0.3$ (GeV:c)$^{-2}$; c) the solution with $\alpha_P(0)>1$ does not exhibit Feynman scaling; d) the growth of $\sigma_D(s)$ at high energies occurs much faster for $\alpha_P(0)>1$ than for $\alpha_P(0)=1$ but it does not completely describe the growth of $\sigma_{tot}(pp)$.

If the values of $G_{PPP}(0)$ and $G_{PPR}(0)$ found in Ref. 115 are used, and if one takes $\sigma_{tot}(pp)\approx 40$ mb and uses Eq. (51), then for the cross section of the pomeron–proton interaction at $t=0$ the following result is obtained:

$$\sigma_{Pp}(M_X^2,\ 0)\approx(0.76+0.46/M_X)\ \text{mb}. \quad (66)$$

To conclude this section, we give the values of the vertices G_{ijk} that can be obtained from the finite-mass sum rules and the DHD model without using data from the region of large masses.[62] Taking into account the relations (54)–(57) and the approximation $Q(t)\approx 9\times\exp(14.5t)$, we obtain the $G_{ijk}(t)$ values shown graphically in Figs. 43 and 44 in the different variants of two-component duality. In the case of normal two-component duality at small $|t|$, the value of G_{PRR} is very small, whereas in the abnormal case G_{PRP} is small. In both cases, the cross terms are large.

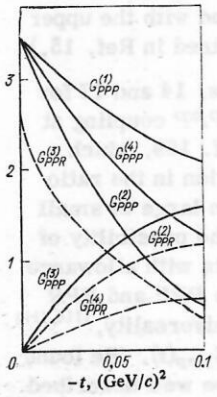

FIG. 44. Diffraction three-reggeon vertices.

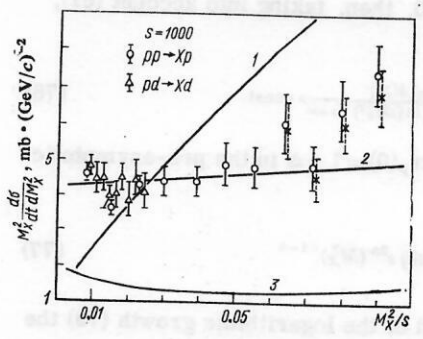

FIG. 45. Comparison with experiment: 1) normal nondiffraction contributions; 2) abnormal nondiffraction+normal diffraction contributions; 3) abnormal nondiffraction+abnormal diffraction contributions.

Let us compare our results with the data at large M_X. We restrict ourselves to the special case $t \to 0$, for which the relations are especially simple. The data on the reactions $pd \to Xd$ and $pp \to Xp$ are extrapolated to $t=0$ in Figs. 45–47. The crosses correspond to extrapolation with exclusion of pion exchanges, which do not contribute to the reaction on deuterium.[62] As can be seen from these figures, in none of the considered cases of extremal duality can one obtain a satisfactory description of experiment in the complete M_X^2/s range. In the framework of the adopted approximations, this means that mixed duality holds for the reggeon–hadron amplitudes. It is important to emphasize that, contrary to the widespread opinion,[86] normal duality is forbidden for the total nondiffraction contribution, although it may hold separately for the PR or RR terms. Vanishing of the three-pomeron coupling as $t \to 0$ is possible in the present approach, which does not take into account the resonance contributions, only in the case of extremal abnormal duality for the $Pp \to Pp$ amplitude. In order to place such predictions on a more reliable basis, it is necessary to use a more realistic DHD model with absorption and cross terms and take into account accurately the contribution of the resonances to the finite-mass sum rules. In this case, the model may give useful bounds on the three-reggeon vertices.

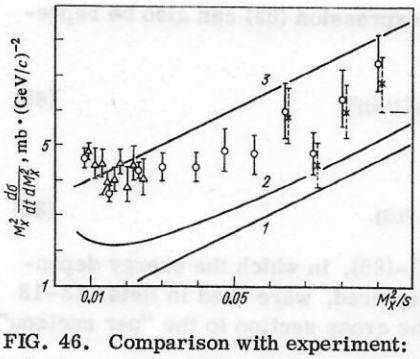

FIG. 46. Comparison with experiment: 1) nondiffraction contributions: normal RR, abnormal PR; 2) curve 1+abnormal diffraction contribution; 3) curve 1+normal diffraction contributions.

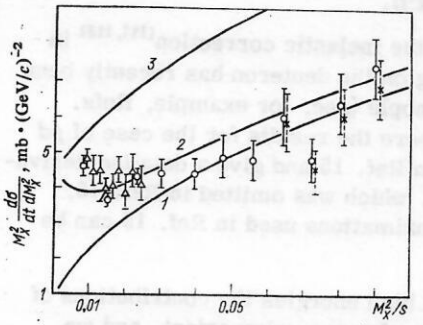

FIG. 47. Comparison with experiment: 1) nondiffraction contributions: normal PR, abnormal RR; 2) curve 1+abnormal diffraction contributions; 3) curve 1+normal diffraction contributions.

Connection between the cross sections of scattering on the nucleon and the deuteron

As we have noted above, the use of deuterium nuclei as targets provides a number of advantages associated with the selection rules and the possibility of obtaining information about the spacetime development of the hadron interactions. To establish the connection between the cross sections of scattering on the nucleon and the deuteron, the Glauber formalism is usually employed.[116]

Let us consider first elastic pd scattering (Fig. 48). The diagram of Fig. 48a takes into account single scattering, whereas Figs. 48b and 48c represent elastic and inelastic screening. Assuming equality of the amplitudes for interaction with the neutron and proton, we write the pd scattering amplitude in the form

$$\left.\begin{aligned} f(t) &= 2f_N(t)\,S(t/4) - \Delta(t), \\ \Delta(t) &= \frac{i}{8\pi^2}\int S(t')\sum_X A(t_1,\ pN \to XN)\,A(t_2,\ XN \to pN)\,dt', \end{aligned}\right\} \quad (67)$$

where

$$t_{1,2} = -(q/2 \pm q')^2;\ t = -q^2; \quad (68)$$

$S(t)$ is the deuteron form factor; $A(t,\ pN \to XN)$ is the amplitude for the production of system X in a pN collision. Assuming $X=N$, we obtain the contribution of elastic screening:

$$\Delta_{el}(t) = i\delta\sigma_{el}\exp(b_{el}t/4). \quad (69)$$

Here, $\delta\sigma_{el} = \sigma_{NN}^2/8\pi(R^2+b_{el})$ is the correction for elastic screening to the total pd cross section, and for the deuteron form factor we have used the exponential param-

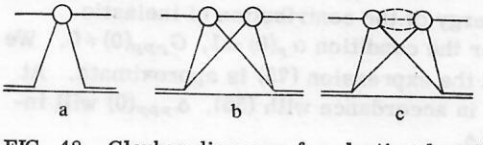

FIG. 48. Glauber diagrams for elastic pd scattering.

etrization $S(t)=\exp(R^2t)$.

The calculation of the inelastic correction[117, 118] in the case of scattering on the deuteron has recently been discussed by many people (see, for example, Refs. 119–121). We give here the results for the case of pd scattering taken from Ref. 15 and give a detailed derivation of these results, which was omitted in Ref. 15, from which the approximations used in Ref. 15 can be clearly seen.

We assume that at high energies the contributions of the secondary Regge poles are unimportant, and we shall take into account in the $A(t,\ pN\to XN)$ amplitude only the contribution of pomeron exchanges. We consider first forward scattering ($t=0$), so that $t_1=t_2$. Using (68) and the results obtained earlier, we can write the contribution of inelastic screening associated with P exchange in the form

$$\Delta_P(0)=2\int dt\,dM_X^2 S(t')\left(\frac{d\sigma}{dt\,dM_X^2}\right)_P. \tag{70}$$

where only the pomeron contribution is taken into account in the dissociation cross section. Parametrizing this cross section at small $|t|$,

$$\left(\frac{d\sigma}{dt\,dM_X^2}\right)_P=\left(\frac{d\sigma}{dtdM_X^2}\right)_{t=0}\exp\left[b_P(M_X)\,t\right], \tag{71}$$

and integrating with respect to t, we obtain

$$\Delta_P(0)=2\int dM_X^2\left(\frac{d\sigma}{dtdM_X^2}\right)_{t=0}\frac{\exp\left[(R^2+b_P(M_X))\,t_{\min}\right]}{R^2+b_P(M_X)}. \tag{72}$$

We divide the region of integration in (72) into the region of small masses $m+\mu<M_X<M_0$, where the peak at $M_X\approx 1.4$ GeV predominates, and into the region of large masses $M_X>M_0$, where the three-reggeon formalism can be used to describe the inclusive cross section. If $M_X<M_0$ and $s\gg M_0^2$, then $t_{\min}\approx 0$, so that

$$\Delta_P^{M_0}(0)\approx 2\int\limits_{(m+\mu)^2}^{M_0^2}\left(\frac{d\sigma}{dt\,dM_X^2}\right)_{t=0}\frac{dM_X^2}{R^2+b_P(M_X)}. \tag{73}$$

In the region $M_X>M_0$ the maximal mass that effectively contributes to the integral (72) is bounded by the condition on the longitudinal momentum component:

$$M_X^2\leqslant M_{\max}^2=s_1/mR. \tag{74}$$

Hence $|t_{\min}|\lesssim R^{-2}\ll 1$. Taking into account the contribution of only the PPP vertex and noting, in agreement with experiment, that $b_P(M_X)\approx\text{const}\equiv b_P$ for $M_X>M_0$, we obtain (under the condition $\alpha_P(0)=1$)

$$\Delta_{PPP}(0)=\left[2G_{PPP}(0)/(R^2+b_P)\right]\left[\ln(p/m)-\ln(RM_0^2/2m)\right]. \tag{75}$$

Thus, we arrive at the well-known result of logarithmic growth with energy of the contribution of inelastic screening under the condition $\alpha_P(0)=1$, $G_{PPP}(0)\neq 0$. We emphasize that the expression (75) is approximate. At high energies, in accordance with (55), $\Delta_{PPP}(0)$ will increase as $\ln\ln p$.

If $G_{PPP}(t)\sim t$ as $t\to 0$, then, taking into account (61), we obtain

$$\Delta_{PPP}(0)\sim\frac{\ln\left[s(1-x_0)\,M_0^{-2}\right]}{R^2+2\alpha_P'(0)\ln(sM_0^{-2})}\xrightarrow[s\to\infty]{}\text{const}. \tag{76}$$

For a pomeron with $\alpha_P(0)=1+\Delta$ in the pre-asymptotic region we have

$$\left(\frac{d\sigma}{dt\,dM_X^2}\right)_{PPP}\approx G_{PPP}(0)\,s^{2\Delta}(M_X^2)^{-1-\Delta} \tag{77}$$

and we obtain instead of the logarithmic growth (75) the power-law growth

$$\Delta_{PPP}(0)\approx G_{PPP}(0)\,s^{\Delta}(s^{\Delta}-1)\,\Delta^{-1}. \tag{78}$$

We now consider $t\neq 0$. To calculate $\Delta_{PPP}(t)$, it is necessary to generalize to the case of arbitrary t_i the three-pomeron vertex $G(t_1, t_2, t_3)$, which is measured in inclusive reactions only for $t_1=t_2=t$ and $t_3=0$. (We recall that a similar problem arises in the calculation of the absorptive corrections in the three-reggeon limit.) We shall use the simplest generalization of the exponential dependence (71), which presupposes complete symmetry of the t dependence on all legs of the PPP vertex:

$$G_{PPP}(t_1, t_2, t_3)=G_{PPP}(0, 0, 0)\exp\left[(b_P/2)(t_1+t_2+t_3)\right]. \tag{79}$$

Then from (72) we obtain

$$\Delta_{PPP}(t)=\Delta_{PPP}(0)\exp(3b_Pt/4). \tag{80}$$

In the region of small $|t|$, the total contribution of elastic and inelastic screening can be represented in the approximate form

$$\Delta(t)=\Delta(0)\exp(\bar{b}t). \tag{81}$$

Then, ignoring the $\Delta^2(t)$ terms, we can write down the expression for the differential cross section of pd scattering:

$$(d\sigma/dt)_{pd\to pd}=(d\sigma/dt)_{pN\to pN}F(t,\ p), \tag{82}$$

where

$$F(t,\ p)=4\left[S(t/4)\right]^2\left[1-\varepsilon\exp(-Bt)\right]; \tag{83}$$

$$\varepsilon=\Delta(0)/\sigma_{pN};\ B=(R^2/2+b_{pN})/2-\bar{b}. \tag{84}$$

Finally, as $t\to 0$ the expression (83) can also be represented in the form

$$F_d(p,\ t)=(\sigma_{pd}/\sigma_{pN})^2\left[\hat{S}(t/4)\right]^2, \tag{85}$$

where

$$\hat{S}(t/4)\approx S(t/4)\exp(\varepsilon Bt/2). \tag{86}$$

The expressions (82)–(86), in which the energy dependence of ε has been ignored, were used in Refs. 13–18 and 108 to convert the cross section to the "per nucleon" value.

We now make some numerical estimates of the

screening corrections. Because of the various approximations made above, these estimates will have a semiquantitative nature.

Above, a simple exponential representation was used for the deuteron form factor. Comparing it with (28) in the limit $t \to 0$, we can take $R^2 \approx 52$ (GeV/c)$^{-2}$. If, however, we determine R^2 from the effective slope in a certain interval $0 \leqslant |t| \leqslant |t_0|$, then $R^2_{eff} = 2(b + ct_0)$, and $R^2_{eff} \approx 40$ (GeV/c)$^{-2}$ for $|t_0| \approx 0.1$ (GeV/c)^2. Further, ignoring the energy dependence of σ_{pN} and b_{pN}, we choose for them the values 40 mb and 10 GeV^{-2}, respectively. Then for the elastic correction $\Delta_{el}(0)$ we obtain 2.5 and 3.1 mb for $R^2 = 52$ and 40 (GeV/c)$^{-2}$, respectively. As in Ref. 15, we shall use the latter of these values. To calculate the inelastic correction, we use the data of Refs. 14 and 17. We shall assume that at the maximal energy achieved in this experiment ($p \approx 400$ GeV/c), virtually the entire peak at $M_X < M_0$ in Fig. 14 is due to the pomeron contribution. Integration of the cross section in the region of the peak gives $\Delta_P^{M_0}(0) \approx 0.5$ mb. In the three-reggeon region $b_P \approx 5$ (GeV/c)$^{-2}$. If for $G_{PPP}(0)$ we use the upper estimate 4.5 mb · (GeV/c)$^{-2}$, we obtain $\Delta_{PPP}(0) \approx (0.2 \ln p - 0.51)$ mb. As we have seen above, the value $G_{PPP}(0) \approx 3$ mb · (GeV/c)$^{-2}$ is more realistic. In this case, $\Delta_{PPP}(0) \approx (0.13 \ln p - 0.34)$ mb. In both cases, the term that does not depend on p is close to $\Delta_P^{M_0}(0)$ and has the opposite sign, so that we can approximately assume these terms to cancel, and

$$\Delta_P(0) \approx \delta \ln p, \tag{87}$$

where $\delta = 0.2$ or 0.13 mb for the cases considered. Note that for $p = 400$ GeV/c this gives 1.2 or 0.8 mb for the inelastic correction and this is already an appreciable fraction of $\Delta_{el}(0)$. Since the contribution of the region $M_X < M_0$ is not very important at high energies, we can ignore the difference in the slopes for $M_X < M_0$ and $M_X > M_0$ and in the limit $t \to 0$ use the approximations (81) and (83):

$$\Delta(0) = \Delta_{el}(0) + \delta \ln p; \quad \varepsilon = \Delta_{el}(0)/\sigma_{pN} + (\delta/\sigma_{pN}) \ln p;$$
$$\bar{b} \approx b_{el}/4 \approx 3/4 b_P \approx 3\ (\text{GeV}/c)^{-2}; \quad B \sim 10 - 12\ (\text{GeV}/c)^{-2}. \tag{88}$$

The correction function $1 - \varepsilon \exp(-Bt)$ calculated for the two momenta $p = 50$ and 200 GeV/c is shown in Fig. 49.

For $t \neq 0$ the correction to the slope parameter of the pd scattering cross section due to screening can be written in the form

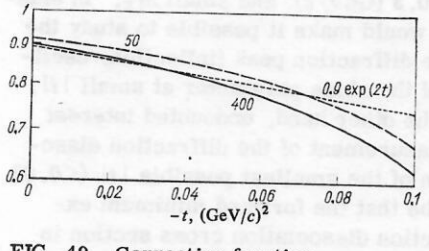

FIG. 49. Correction function.

$$\Delta b = \frac{d}{dt} \ln [1 - \varepsilon \exp(-Bt)] = \frac{B\varepsilon \exp(-Bt)}{1 - \varepsilon \exp(-Bt)}, \tag{89}$$

whence for the energy-dependent part Δb_1 of the correction we obtain

$$\Delta b_1 \approx \frac{B\delta}{\sigma_{pN}} \frac{\exp(-Bt)}{1 - (\Delta_{el}(0)/\sigma_{pN}) \exp(-Bt)}. \tag{90}$$

For $t \approx 0.1$ (GeV/c)^2

$$\Delta b_1 \approx (0.15 \ln p)\ (\text{GeV}/c)^{-2}. \tag{91}$$

In the region $p \approx 200$–400 GeV/c and $0 \leqslant |t| \leqslant 0.1$ (GeV/c)^2, to which the majority of the data in refs. 14, 17, and 18 refer, the approximation $1 - \varepsilon \exp(-Bt) \approx 0.9 \times \exp(2t)$, shown in Fig. 49 by the dashed curve, can be used. It is this result that was given in Ref. 15. Allowance for the energy dependence of the inelastic screening (91) makes it possible to explain the difference observed experimentally between the rates of contraction of the pp and pd scattering peaks. This fact was also noted in Ref. 122.

The equations derived above are based on Glauber theory. At the present time it is not very clear to what extent this formalism is applicable at high energies, in which the spacetime extension of hadron events may be appreciable. In the multiperipheral picture, if the incident particle is to interact (through Regge exchange) with the target it must emit slower particles (partons) at distances $\sim p_z/\mu^2$ from the target. If these distances exceed the nuclear dimensions, we can no longer use the ordinary theory of multiple scattering. Nevertheless, as comparison of the above estimates with experiment shows, one may hope that, at least at accelerator energies, the Glauber formalism can be used provided inelastic intermediate states are taken into account.

In the calculation of the $pd \to Xd$ reaction cross section, a difficulty arises due to our ignorance of the amplitude of rescattering of the excited system X on the nucleon. It is well known that the simplest assumption that this cross section is equal to the sum of the cross sections for the interaction with the nucleon of the decay products of system X is completely false. Already the first experiments on coherent production on nuclei showed that $\sigma_{XN} \approx \sigma_{hN}$, where h is the incident hadron. Recent measurements[123] have found that the complicated spin structure of the cross section of diffraction dissociation leads to a significant difference in the cross sections for interaction of the different spin–parity states in X. The absence of detailed information about the (peripheral) profiles of these states renders unrealistic at the present time any attempt at an accurate calculation of the amplitude for the process. In this connection, it is a very attractive idea to use information about the interaction of the system X deduced directly from experiments, i.e., by comparing the cross sections of the reactions on the nucleon and the deuteron (or another nucleus). Unfortunately, in the kinematic region in which we are interested, data on the $pp \to Xp$ reaction are still very sparse. As we have seen in Sec. 1, at small M_X the data of Bartenev *et al.*[12] agree within the experimental errors with the data on the $pd \to Xd$

reaction if it is assumed that Eq. (82) can be used for diffraction dissociation, i.e., if the XN and NN interactions are similar. At large M_X in the region of small $|t|$ there are only chamber data, which have a relatively large statistical error. Comparison with these lastly shows that the "per nucleon" cross section deduced from the deuteron data is somewhat smaller than the value found in chambers. This can be regarded as an indication of the large relative importance of the Glauber correction in the case of diffraction dissociation compared with the correction for elastic pd scattering. A similar conclusion was also drawn in Ref. 114 from a comparison of the $pd \to Xd$ data[117] with the results of analysis of the $pp \to Xp$ data at large $|t|$.

For a more detailed study of this question, we need data on the reaction $pp \to Xp$ in the same kinematic region as for $pd \to Xd$. Note that the comparison of the proton and deuteron cross sections by means of the relation (82) can be regarded as a verification of "nuclear factorization". Obviously, such factorization must be satisfied to at least the accuracy resulting from neglect of the Glauber corrections,[3)] which in the region of small $|t|$ are 10–20% in the differential cross section. As we have already noted, factorization is indeed observed experimentally within these limits.

CONCLUSIONS

We now formulate the main conclusions drawn from our study.

1. The experiments have shown that at high energies and small $|t|$ in the region $5\ (\text{GeV})^2 \leq M_X^2 \leq 0.05s$ the cross section depends weakly on the energy and decreases with increasing mass as M_X^{-2}. In the framework of Regge theory, this means that the three-pomeron contribution at small $|t|$ is important. A certain indication of departure from scaling is found.

2. Measurement of the t dependence down to very small $|t|$ ($\sim 0.03\ (\text{GeV}/c)^2$) showed that there is no decrease at all of the cross section as $|t|$ decreases. Analysis of the data in terms of three-reggeon interactions leads to the conclusion that the three-pomeron (effective) vertex does not become zero in the limit $t \to 0$.

3. The good mass resolution has made it possible to follow the motion of the "threshold dip" in the cross section as a function of the energy and thus confirm experimentally the increase in the diffraction dissociation cross section with increasing energy. The increase found is insufficient to explain the growth of the total pp scattering cross section.

4. For the first time in experiments at high energies a resonance structure of the diffraction dissociation in the region of small masses has been found. The peak in the nucleon dissociation mass spectrum at small M_X evidently contains appreciable contributions of nonresonance threshold mechanisms of the DHD type and resonance contributions interferring with them.

5. Comparison of the data on elastic pp and pd scattering has shown that Glauber theory with allowance for inelastic screening can be used right up to $p \approx 400$ GeV/c. Comparison of the analogous data for diffraction dissociation revealed an indication of a difference in the Glauber correction for elastic and inelastic reactions. Nuclear factorization holds to within ~20%. The more rapid contraction of the pd elastic scattering peak compared with that for pp scattering can be explained by the energy dependence of the correction for inelastic screening, which at high energies is due primarily to three-pomeron interaction.

6. For the cross section of pomeron–proton interaction in different variants of the Regge model the estimate $\sigma_{Pp}(t=0) \approx 1-2$ mb is obtained, and for the three-pomeron vertex $G_{PPP}(0) \approx 1.5-3\ \text{mb}(\text{GeV}/c)^{-2}$.

7. Comparison of the diffraction dissociation cross sections at small and large M_X indicates that mixed duality, in which the pomeron contribution is dual to the resonances and nonresonance background, holds for the amplitudes of reggeon–nucleon scattering.

8. In diffraction dissociation processes, an important role is played by absorptive effects, which lead to some important consequences at both small and large M_X. The strong absorption at small impact parameters leads to a peripheral diffraction dissociation profile. As a consequence, small-scale oscillations arise in the differential cross section of elastic scattering. The absorptive corrections significantly reduce the value of the cross section. As a result, the bare three-pomeron vertex may be several times larger than the effective vertex deduced from the experiment. A reliable estimate of the absorptive effects is one of the most important tasks of the theory, and without it it is impossible to solve the problem of finding the true ("bare") three-reggeon vertices, which play an important role in the theory of strong interactions at high energies.

The use of the jet target provides great possibilities for continuing investigations into diffraction dissociation. The first tasks to be tackled are those of obtaining data on the reaction $pp \to Xp$ in the region of large M_X and small $|t|$ and comparing them with the data obtained on deuterium. Measurements on ^{4}He can also give additional interesting information.[35] It is also important to extend the range of measurements with respect to t in order to render possible a direct comparison with the data of other experiments, in particular, the data obtained on the colliding beams at CERN. The region of large $|t|$ is also interesting from the point of view of studying the minimum in the diffraction dissociation differential cross section found in the exclusive channels at $t \approx 0.2-0.3\ (\text{GeV}/c)^2$ and small M_X. In elastic scattering, this would make it possible to study the fine structure of the diffraction peak (inflection, oscillations, decrease of the slope parameter at small $|t|$, and so forth). On the other hand, undoubted interest also attaches to measurement of the diffraction dissociation in the region of the smallest possible $|t|$ ($< 0.03\ (\text{GeV}/c)^2$). It may be that the forward minimum expected in the diffraction dissociation cross section in

---

[3)] In this approximation, to accuracy Δ_{el} since Δ_{PPP} factorizes.

the model with $G_{PPP}(0) = 0$ appears only at very small $|t|$. In this same region, it would be interesting to discover a manifestation of interference with Coulomb dissociation. The rich spin structure of diffraction dissociation also promises interesting polarization effects. Finally, detection of more than one particle in the final state would undoubtedly extend the possibilities of this experimental method.

Finally, we must express our gratitude to the State Committee for the Utilization of Atomic Energy in the USSR and the Energy Research and Development Administration in the United States for making possible these joint experiments, to the Directors of the Joint Institute for Nuclear Research, the High Energy Laboratory at Dubna, and the Fermi National Accelerator Laboratory and especially to N. N. Bogolyubov, A. M. Baldin, and R. R. Wilson for constant support and interest in the joint work; to our colleagues at Dubna and Fermilab with whom the experiments were made on which the present work is based and the personnel on the American side for hospitality and creating the conditions for successful carrying out of the experiments. We also thank A. M. Baldin, V. A. Nikitin, L. I. Lapidus, and B. Z. Kapilovich for helpful discussion during the preparation of this paper.

[1]M. G. Albrow *et al.*, Nucl. Phys. B **51**, 388 (1973); **72**, 376 (1974).
[2]E. L. Feinberg, J. Phys. **5**, 177 (1941); E. L. Feinberg and I. Pomerančhuk, Suppl. Nuovo Cimento **3**, 652 (1956); R. J. Glauber, Phys. Rev. **99**, 1515 (1955); E. L. Feĭnberg, Zh. Eksp. Teor. Fiz. **29**, 115 (1955) [Sov. Phys. JETP **2**, 58 (1956)]; A. I. Akhiezer and A. G. Sitenko, Phys. Rev. **106**, 1236 (1957); A. I. Akhiezer and A. G. Sitenko, Dokl. Akad. Nauk SSSR **107**, 385 (1956) [Sov. Phys. Doklady **1**, 180 (1956)]; A. I. Akhiezer and A. G. Sitenko, Zh. Eksp. Teor. Fiz. **32**, 794 (1957) [Sov. Phys. JETP **5**, 652 (1957)]; A. G. Sitenko and Ya. A. Berezhnoĭ, Zh. Eksp. Teor. Fiz. **35**, 1289 (1958) [Sov. Phys. JETP **8**, 899 (1959)]; J. S. Blair, Nucl. Phys. **6**, 348 (1958); G. P. Millburn *et al.*, Phys. Rev. **95**, 1268 (1954).
[3]M. L. Good and W. D. Walker, Phys. Rev. **120**, 1857 (1960).
[4]S. V. Mukhin and V. A. Tsarev, in: Proc. of the 1974 Williamsburg Meeting of the Division of Particles and Fields of the A.P.S. (Ed. C. E. Carlson), American Institute of Physics, New York (1975), p. 263.
[5]I. M. Gramenitskiĭ and Z. Novak, Fiz. Elem. Chastits At. Yadra **5**, 63 (1974) [Sov. J. Part. Nucl. **5**, 25 (1974)].
[6]A. V. Kaĭdalov and V. A. Khoze, Preprint LIYaF No. 193 Leningrad Inst. of Nucl. Phys., [in Russian] (1975).
[7]M. Derrick, Preprint ANL-HEP-CP-75-52 (1975).
[8]H. I. Miettinen, in: Proc. of the E.P.S. Intern. Conf. on High Energy Physics, Palermo (1975) (Ed. A. Zichichi), Bologna (1976), p. 731.
[9]G. Cohen-Tannoudji, A Morel, and P. Strolin, in: Proc. École été de Physique des particules (1975), p. 79.
[10]D. W. G. S. Leith, Preprint SLAC-PUB-1646 (1975).
[11]U. Amaldi, M. Jacob, and G. Matthiae, Ann. Rev. Nucl. Sci. **26**, 385 (1976).
[12]V. Bartenev *et al.*, Phys. Lett. B **51**, 299 (1974).
[13]Y. Akimov *et al.*, Fermilab-Conf.-74/56-exp., London (1974).
[14]Y. Akimov *et al.*, Fermilab-Conf.-74/66-exp., London (1974).
[15]Y. Akimov *et al.*, Fermilab-Conf.-74/79-exp., London (1974).
[16]Y. Akimov *et al.*, Phys. Rev. Lett. **35**, 763 (1975).
[17]Y. Akimov *et al.*, Phys. Rev. Lett. **35**, 766 (1975).
[18]Y. Akimov *et al.*, Paper N 1262, submitted to the Eighteenth Intern. Conf. on High Energy Physics, Tbilisi (1976).
[19]J. C. Sens, Topics in Particle Physics at ISR, Lectures, 1973; Acad. Press, London-New York (1974).
[20]V. A. Nikitin *et al.*, Prib. Tekh. Eksp, No. 6, 18 (1963).
[21]V. A. Nikitin *et al.*, Zh. Eksp. Teor. Fiz. **46**, 1608 (1964) [Sov. Phys. JETP **19**, 1088 (1964)].
[22]Yu. K. Akimov *et al.*, Zh. Eksp. Teor. Fiz. **48**, 767 (1965) [Sov. Phys. JETP **21**, 507 (1965)].
[23]Yu. K. Akimov *et al.*, Yad. Fiz. **4**, 88 (1966) [Sov. J. Nucl. Phys. **4**, 63 (1967)].
[24]V. D. Bartenev *et al.*, in: Trudy Mezhdunarodnoĭ Konferentsii po Apparature v Fizike Vysokikh Énergiĭ (Proc. Intern. Conf. on Apparatus in High Energy Physics), Dubna (1970), p. 16.
[25]G. G. Beznogikh *et al.*, Phys. Lett. B **39**, 411 (1972).
[26]V. D. Bartenev *et al.*, Preprint JINR R13-6324 [in Russian], Dubna (1972).
[27]V. Bartenev *et al.*, Adv. Cryog. Eng. **18**, 460 (1973).
[28]V. Bartenev *et al.*, Phys. Rev. Lett. **31**, 1088 (1973).
[29]V. Bartenev *et al.*, Phys. Rev. Lett. **31**, 1367 (1973).
[30]K. Abe *et al.*, Phys. Rev. Lett. **31**, 1527 (1973).
[31]F. Sannes *et al.*, Phys. Rev. Lett. **30**, 766 (1973).
[32]V. A. Nikitin, Fiz. Elem. Chastits At. Yadra **1**, 7 (1970) [Particles and Nuclei **1**, part 2, 2 (1970) (Plenum Press)].
[33]M. G. Shafranova, Fiz. Elem. Chastits At. Yadra **5**, 645 (1974) [Sov. J. Part. Nucl. **5**, 259 (1974)].
[34]Y. Akimov *et al.*, Phys. Rev. D **12**, 3399 (1975).
[35]E. Malamud *et al.*, FNAL proposal 289.
[36]R. Schamberger *et al.*, Submitted to the APS Division of Particles and Fields Meeting, Berkeley, August 1973).
[37]S. Childress *et al.*, Paper Submitted to the APS Division of Particles and Fields Meeting, Berkeley, August (1973).
[38]J. Whitmore *et al.*, Phys. Lett. B **50**, 280 (1974).
[39]J. Whitmore *et al.*, Phys. Rev. D **11**, 3124 (1974).
[40]M. G. Albrow *et al.*, Phys. Lett. B **42**, 279 (1972).
[41]M. G. Albrow *et al.*, Nucl. Phys. B **108**, 1 (1976).
[42]W. F. Baker *et al.*, Phys. Rev. Lett. **33**, 928 (1974).
[43]E. W. Anderson *et al.*, Phys. Rev. Lett. **16**, 855 (1966).
[44]R. M. Edelstein *et al.*, Phys. Rev. D **5**, 1073 (1972).
[45]J. V. Allaby *et al.*, Nucl. Phys. B **52**, 316 (1973).
[46]P. H. Frampton and P. V. Ruuskanen, Phys. Lett. B **38**, 78 (1972).
[47]G. Bellettini *et al.*, Phys. Lett. **18**, 167 (1965).
[48]E. Nagy *et al.*, Paper Submitted to 17th Intern. Conf. on High Energy Physics, London (1974).
[49]S. Childress *et al.*, Paper 829 Submitted to the 18th Intern. Conf. on High Energy Physics, Tbilisi (1976); Phys. Lett. B **65**, 177 (1976).
[50]J. C. M. Armitage *et al.*, Paper 345 Submitted to the 18th Intern. Conf. on High Energy Physics, Tbilisi (1976).
[51]T. Ferbel, in: Proc. of the E.P.S. Intern. Conf. on High Energy Physics, Palermo, 1975, (Ed. A. Zichichi), Bologna (1976), p. 921.
[52]V. A. Tsarev, Phys. Rev. D **11**, 1864 (1975).
[53]V. Blobel *et al.*, Preprint MPI-Exp-EI-49 (1975).
[54]V. Blobel *et al.*, Nucl. Phys. B **69**, 454 (1974).
[55]K. Boesebeck *et al.*, Nucl. Phys. B **33**, 445 (1971).
[56]C. Białas, W. Czyż, and A. Kotański, Ann. Phys. (N.Y.) **73**, 439 (1972).
[57]M. Ross and Y. Y. Yam, Phys. Rev. Lett. **19**, 546 (1967); Phys. Rev. Lett. **19**, 940 (1967).
[58]S. D. Drell and K. Hiida, Phys. Rev. Lett. **7**, 199 (1961).
[59]R. T. Deck, Phys. Rev. Lett. **13**, 169 (1964).
[60]L. A. Ponomarev, Fiz. Elem. Chastits At. Yadra **7**, 186 (1976) [Sov. J. Part. Nucl. **7**, 70 (1976)].
[61]L. Stodolsky, Phys. Rev. Lett. **18**, 973 (1967).
[62]V. A. Tsarev, Phys. Rev. D **11**, 1875 (1975).
[63]E. L. Berger and P. Pirilä, Phys. Rev. D **12**, 3448 (1975).

[64]J. Biel *et al.*, Phys. Rev. Lett. **36**, 504 (1976).
[65]N. I. Starkov and V. A. Tsarev, Pis'ma Zh. Eksp. Teor. Fiz. **23**, 403 (1976) [JETP Lett. **23**, 363 (1976)].
[66]C. Sorensen, Phys. Rev. D **6**, 2554 (1972).
[67]R. T. Cutler and H. W. Wyld, Phys. Rev. D **12**, 1952 (1975).
[68]E. L. Berger, Report DL/R34, Daresbury (1975).
[69]M. Uehara, Preprint KYUSHU-76-YE-2 (1976).
[70]A. Babaev *et al.*, Nucl. Phys. B **116**, 28 (1976).
[71]P. Söding, Phys. Lett. **19**, 702 (1965); M. G. Bowler *et al.*, Nucl. Phys. B **97**, 227 (1975).
[72]O. V. Kancheli, Pis'ma Zh. Eksp. Teor. Fiz. **11**, 397 (1970); [JETP Lett. **11**, 267 (1970)]; A. M. Mueller, Phys. Rev. D **2**, 2963 (1970).
[73]R. Shankar, Preprint LBL-2678 (1974).
[74]L. A. P. Balázs, Phys. Rev. D **11**, 1071 (1975).
[75]M. Bishari, Phys. Lett. B **38**, 510 (1972).
[76]A. A. Logunov, L. D. Soloviev, and A. N. Tavkhelidze, Phys. Lett. B **24**, 181 (1967).
[77]K. Igi and S. Matsuda, Phys. Rev. Lett. **18**, 625 (1967).
[78]R. Dolen, D. Horn, and C. Schmid, Phys. Rev. Lett. **19**, 402 (1967).
[79]Y. C. Liu and S. Okubo, Phys. Rev. Lett. **19**, 190 (1967).
[80]J. Kwieciński, Nuovo Cimento Lett. **3**, 619 (1972).
[81]A. I. Sanda, Phys. Rev. D **6**, 280 (1972).
[82]M. B. Einhorn, J. E. Ellis, and J. Finkelstein, Phys. Rev. D **5**, 2063 (1972).
[83]P. G. O. Freund, Phys. Rev. Lett. **20**, 235 (1968).
[84]H. Harari, Phys. Rev. Lett. **20**, 1395 (1968).
[85]M. B. Einhorn, in: Proc. 16th Intern. Conf. on High Energy Physics, Vol. 1, Chicago-Batavia (1972), p. 417.
[86]P. Hoyer, in: Proc. 17th Intern. Conf. on High Energy Physics, London (1974), pp. 1–158.
[87]M. B. Einhorn, M. B. Green, and M. A. Virasoro, Phys. Lett. B **37**, 292 (1971).
[88]S.-H. H. Tye and G. Veneziano, Phys. Lett. B **38**, 30 (1972).
[89]H. D. I. Abarbanel *et al.*, Ann. Phys. (N.Y.) **73**, 156 (1972).
[90]T. Gaisser and C. I. Tan, Phys. Rev. D **8**, 3881 (1973).
[91]M. Suzuki, Nucl. Phys. B **64**, 486 (1973).
[92]V. N. Gribov and A. A. Migdal, Yad. Fiz. **8**, 1002 (1968) [Sov. J. Nucl. Phys. **8**, 583 (1969)].
[93]V. N. Gribov, Yad. Fiz. **17**, 603 (1973) [Sov. J. Nucl. Phys. **17**, 313 (1973)].
[94]A. A. Migdal, A. M. Polyakov, and K. A. Ter-Martirosyan, Phys. Lett. B **48**, 239 (1974)].
[95]H. D. I. Arbarbanel and J. B. Bronzan, Phys. Lett. B **48**, 345 (1974).
[96]H. Cheng and T. T. Wu, Phys. Rev. Lett. **24**, 1456 (1970).
[97]M. S. Dubovikov and K. A. Ter-Martirosyan, Preprint ITEP-37 (1976); B. Z. Kopeliovich and L. I. Lapidus, Zh. Eksp. Teor. Fiz. **71**, 61 (1976) [Sov. Phys. JETP **44**, 31 (1976)]; M. S. Dubovikov *et al.*, Preprint JINR D2-9789 [in Russian], Dubna (1976).
[98]D. Amati *et al.*, Preprint TH-2152 CERN (1976).
[99]A. Capella and A. Kaidalov, Preprint TH 2151-CERN (1976).
[100]A. Capella, J. Kaplan, and Tran. Thanh Van, Nucl. Phys. B **105**, 333 (1976).
[101]N. Sakai and J. N. J. White, Nucl. Phys. B **59**, 511 (1973).
[102]J. Pumplin, Phys. Rev. D **8**, 2899 (1973).
[103]L. Caneschi *et al.*, Phys. Lett. B **56**, 359 (1975).
[104]V. A. Tsarev, in: Talk at 18th Intern. Conf. on High Energy Physics, Tbilisi (1976).
[105]V. A. Tsarev, Preprint NAL-Pub-74/17 (1974).
[106]Yu. M. Antipov *et al.*, Paper No. 40, Presented at 18th Intern. Conf. on High Energy Physics, Tbilisi (1976).
[107]V. G. Ableev *et al.*, Paper No. 447, Presented at 18th Intern. Conf. on High Energy Physics, Tbilisi (1976).
[108]Y. Akimov *et al.*, Fermilab-Pub-76/36 (1976).
[109]A. G. Azkarate, Nuovo Cimento **32**, 65 (1976).
[110]R. Carlitz, M. B. Green, and A. Zee, Phys. Rev. D **4**, 3439 (1971).
[111]G. F. Chew and D. R. Snider, Phys. Rev. D **3**, 420 (1971).
[112]R. D. Field and G. C. Fox, Nucl. Phys. B **80**, 367 (1974).
[113]L. G. Dakhno, Yad. Fiz. **23**, 862 (1976) [Sov. J. Nucl. Phys. **23**, 454 (1976)].
[114]Yu. M. Kazarinov *et al.*, Zh. Eksp. Teor. Fiz. **70**, 1152 (1976) [Sov. Phys. JETP **43**, 598 (1976)].
[115]S. Y. Chu, B. R. Desai, B. C. Shen, and R. D. Field, Preprint UCR-75-03 (1975).
[116]R. J. Glauber, Phys. Rev. **100**, 242 (1955).
[117]J. Pumplin and M. Ross, Phys. Rev. Lett. **21**, 1778 (1968).
[118]V. N. Gribov, Zh. Eksp. Teor. Fiz. **56**, 892 (1969) [Sov. Phys. JETP **29**, 483 (1969)].
[119]A. B. Kaidalov and L. A. Kondratyuk, Nucl. Phys. B **56**, 90 (1973).
[120]J. Kwieciński, L. Leśniak, and K. Zalewski, Nucl. Phys. B **78**, 251 (1974).
[121]V. V. Anisovich and L. G. Dakhno, Nucl. Phys. B **85**, 208 (1975).
[122]Yu. I. Azimov *et al.*, Pis'ma Zh. Eksp. Teor. Fiz. **23**, 131 (1976) [JETP Lett. **23**, 114 (1976)].
[123]W. Beusch *et al.*, Phys. Lett. B **55**, 97 (1975).

Translated by Julian B. Barbour